frontiers | Frontiers in Materials

TYPE Review
PUBLISHED 06 March 2023
DOI 10.3389/fmats.2023.1133287

OPEN ACCESS

EDITED BY
Guilherme Mariz de Oliveira Barra,
Federal University of Santa Catarina,
Brazil

REVIEWED BY
Yassine Slimani,
Imam Abdulrahman Bin Faisal University,
Saudi Arabia
Hualiang Lv,
The Ohio State University, United States

*CORRESPONDENCE
Reza Peymanfar,
reza_peymanfar@alumni.iust.ac.ir
Hossein Ghafuri,
ghafuri@iust.ac.ir

SPECIALTY SECTION
This article was submitted to Polymeric and Composite Materials, a section of the journal *Frontiers in Materials*

RECEIVED 28 December 2022
ACCEPTED 16 February 2023
PUBLISHED 06 March 2023

CITATION
Peymanfar R, Dogari H, Selseleh-Zakerin E, Hedayatzadeh MH, Daneshvar S, Amiri-Ramsheh N, Ghafuri H, Mirkhan A, Ji G and Aslibeiki B (2023), Recent advances in microwave-absorbing materials fabricated using organic conductive polymers. *Front. Mater.* 10:1133287. doi: 10.3389/fmats.2023.1133287

Recent advances in microwave-absorbing materials fabricated using organic conductive polymers

Reza Peymanfar[1,2,3]*, Haniyeh Dogari[4], Elnaz Selseleh-Zakerin[1], Mohammad Hossein Hedayatzadeh[4], Sara Daneshvar[4], Nasim Amiri-Ramsheh[4], Hossein Ghafuri[4]*, Ali Mirkhan[2,3], Guangbin Ji[5] and Bagher Aslibeiki[6]

[1]Department of Health Safety and Environment (HSE), Energy Institute of Higher Education, Saveh, Iran, [2]Department of Science, Iranian Society of Philosophers, Tehran, Iran, [3]Peykareh Enterprise Development Co., Tehran, Iran, [4]Catalysts and Organic Synthesis Research Laboratory, Department of Chemistry, Iran University of Science and Technology, Tehran, Iran, [5]College of Materials Science and Technology, Nanjing University of Aeronautics and Astronautics, Nanjing, China, [6]Faculty of Physics, University of Tabriz, Tabriz, Iran

Microwave-absorbing materials are widely utilized in military and civilian applications. Moreover, their environmental potential to refine electromagnetic pollution has promoted their importance. An ideal conjugated organic polymer for use as a microwave-absorbing material should possess high porosity, low density, a long conjugated backbone, a narrow energy band gap, proper conductive and relaxation loss, and vast specific surface area. This review describes the conductive polymer types used as microwave-absorbing material and their composites toward improving microwave-absorbing capability. Additionally, recent developments in synthetic strategies and structural properties of pure carbon-based microwave-absorbing materials and other conjugated structures having heteroatoms in their chains are discussed. In the field of microwave absorbers, the predominant microwave-absorbing mechanisms among conductive polymers and their composites as well as the special mechanisms for tuning microwave-absorbing characteristics, including metamaterial and quasi-antenna features, are dissected. This review sheds new light on architecting low-density and high-performance microwave-absorbing structures and offers new prospects in tailoring conjugated polymers based on their dominant mechanisms.

KEYWORDS

conductive polymer, microwave-absorbing materials, dielectric structures, conjugated polymer, metamaterial, quasi-antennas

1 Introduction

Microwave-absorbing materials play a crucial role in preserving human and environmental health by controlling and reducing electromagnetic pollution (Peymanfar et al., 2021a; Lv et al., 2021; Cheng et al., 2022; Lei et al., 2022; Lou et al., 2022). The vital factors mitigating microwaves are magnetic and dielectric losses by converting electromagnetic energy to heat energy (Peymanfar and Fazlalizadeh, 2021;

Yang et al., 2022a). Accordingly, massive efforts have been made to architect microwave-absorbing material to protect against electromagnetic pollution.

Recently, scientists have focused on architecting high-performance microwave-absorbing materials with a broad efficient bandwidth and strong absorption properties. Many studies have reported on metal nanoparticles, ceramics, and conductive polymers, considered the principal components of electromagnetic wave-absorbing materials in the matrix (Li et al., 2019; Li et al., 2022; Lv et al., 2022). An ideal microwave-absorbing structure has a broad bandwidth, low matching thickness, lightweight and affordable properties, strong absorption, and facile experimental scenarios. A practical microwave-absorbing structure should have dielectric and magnetic characteristics to allow proper impedance matching. By establishing natural and exchange resonance, magnetic structures amplify the permeability desirable for electromagnetic attenuation (Zhang et al., 2021a). The presence of heteroatoms in conductive polymers provides permeability by creating metamaterial features (Peymanfar et al., 2020a; Peymanfar et al., 2020b; Peymanfar and Fazlalizadeh, 2021; Peymanfar et al., 2022). Polyaniline, polythiophene, polypyrrole, and polydopamine are the pioneer and effective conductive polymers that feature heteroatoms in their backbones and are used in fabricating microwave-absorbing components (Das and Prusty, 2012; Wang, 2014; Wang et al., 2017; Peymanfar et al., 2019a; Peymanfar et al., 2020a; Peymanfar et al., 2020b; Xue et al., 2020; Peymanfar et al., 2021b; Soares et al., 2021; Peymanfar et al., 2022). Moreover, the size and shape of electromagnetic absorbers influence the tuning of microwave-absorbing characteristics by enhancing polarization loss and establishing secondary fields (Peymanfar et al., 2018; Peymanfar and Fazlalizadeh, 2021). The energy band gap, a crucial factor regulating conductive and dielectric loss characteristics, is tuned by modifying the nanostructure shape (Peymanfar et al., 2018; Peymanfar et al., 2020c; Peymanfar and Fazlalizadeh, 2020; Peymanfar et al., 2021c).

Morphological change in conjugated conducting polymers can also change the orbital orientations to modulate conductive loss and multiple reflections and scatterings and alter the path of electron transmission and penetration to tune relaxation loss (Ding et al., 2012; Yan et al., 2018; Peymanfar et al., 2020c; Peymanfar and Fazlalizadeh, 2020; Guan et al., 2021). Conjugated organic substances have high dielectric loss capabilities. Three reported methods can be used to improve the dielectric loss capability of this class of materials: 1) enhancing the specific surface area by augmenting the porosity, increasing the surface area-to-volume ratio desirable for polarization loss, and eventually reducing the density by diminishing the filler amount; 2) compositing the conductive polymers with functional materials to enhance impedance matching, establish permeability, and promote other essential microwave-absorbing mechanisms; and 3) doping the materials with heteroatoms: establishing unpaired spins and regulating conductive loss, generating magnetic order, developing dipole polarization, improving quasi-antenna characteristics and impedance matching, and tuning the energy band gap (Zhao et al., 2016).

Recently, new materials, known as metamaterials, have been identified, which have attracted attention for electromagnetic wave absorption as well as optical and plasmonic fields. Metamaterials have inverse electromagnetic responses with remarkable absorption. Metamaterials provide electric and magnetic resonances, boosting impedance matching and maximizing reflection loss by augmenting the propagation of incident waves in the absorbing medium (Ding et al., 2012). More interestingly, the polarized structures under the alternating fields can act as quasi-antennas, resulting in secondary fields and metamaterial features (Yan et al., 2018).

This review evaluated the microwave-absorbing ability of various types of conjugated conductive polymers. The synthesis routes, structural characteristics, and microwave-absorbing mechanisms of this type of material were highlighted to pave the way for future research. Subsequently, recent developments in the field of quasi-antenna and metamaterial characteristics related to conducting organic polymers were discussed. Finally, state-of-the-art research in conductive polymers was highlighted and the horizon of cutting-edge microwave-absorbing developments was broadened by investigating the mechanisms of the microwave-absorbing capability of conjugated organic polymers and related structures as well as their structural properties to generate lightweight and high-performance absorbers.

2 Microwave-absorbing materials fabricated by conductive polymers

Organic conductive polymers are constructed based on pure conjugated carbon and carbonaceous structures with heteroatoms in their polymeric backbone. The facile charge transitions from π to π^* and from n to π^* provide their salient conductive and dielectric losses along the SP^2 hybridization. The morphology, defects, orbital orientation, chain length, and remaining functional groups of the pure carbon-based conductive polymers define their microwave-absorbing performance, while the orbital orientation, guest electronegativity, defects, morphology, chain length, and non-bonding electrons on the hetero atoms associated with other types of organic conductive polymers clarify their electromagnetic responses.

Conductive polymer structures have attracted attention in the field of energy conversion and storage due to their excellent electrical characteristics. The microwave-absorbing performances of the conjugated polymers are strongly affected by their chemical structures, orbital orientations, and morphologies. Elemental doping, as well as dielectric and magnetic components, has been applied to enhance microwave-absorbing features and achieve synergistic effects. This review discusses recent advances in conductive polymer structures composed of conjugated carbon and other organic polymers with heteroatoms. The microwave-absorbing properties of the materials are estimated according to their complex permittivity ($\varepsilon_r = \varepsilon' - j\varepsilon''$) and permeability ($\mu_r = \mu' - j\mu''$) to establish impedance matching. The prime notation refers to the storage ability, while the double-prime notation indicates the attenuation capacity of an absorber. The microwave absorption potential is examined based on the reflection loss (RL) curves obtained by the transmission line theory. Figure 1 presents an

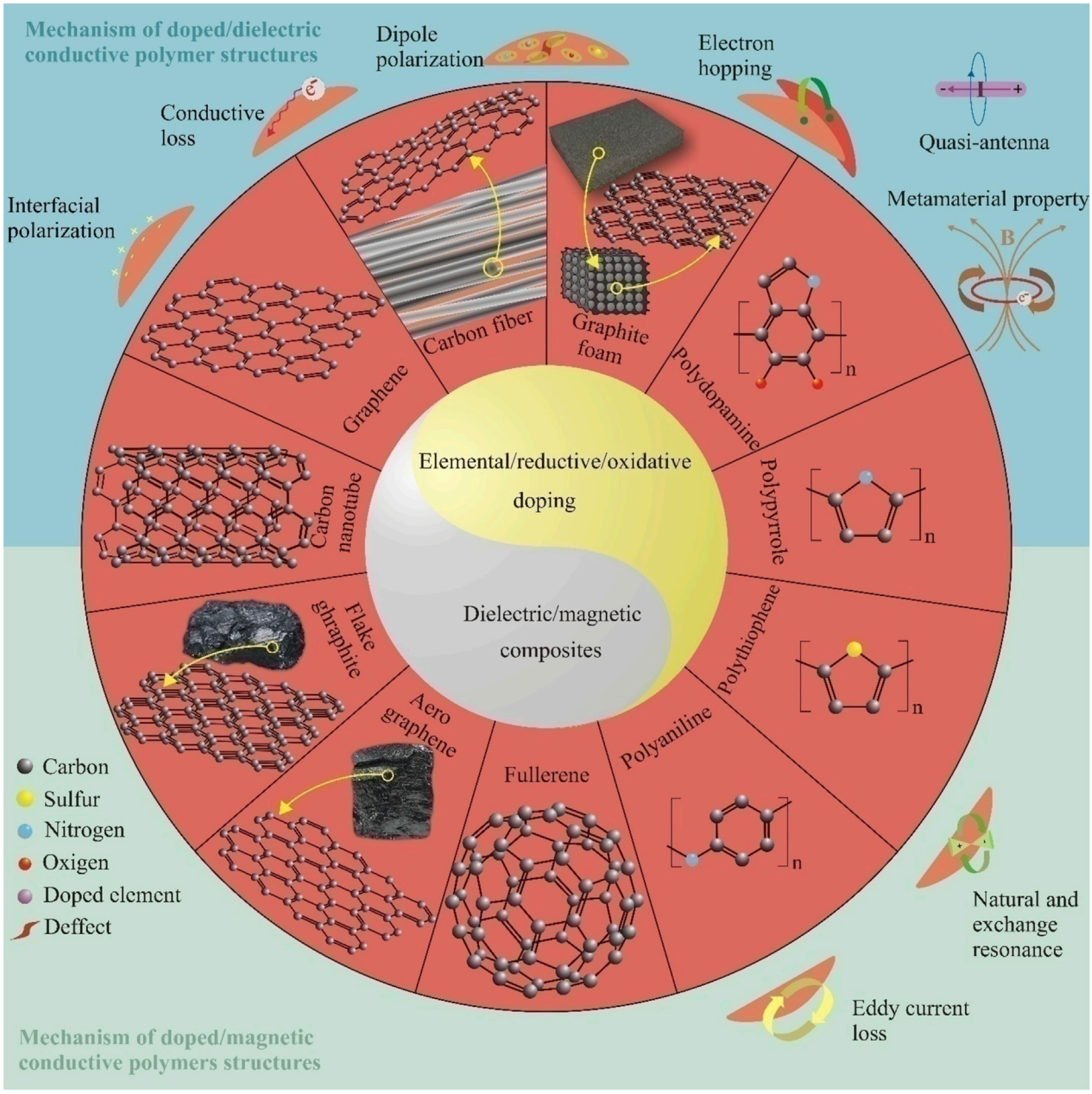

FIGURE 1
Schematic diagram of conductive polymer-based microwave-absorbing materials and the related microwave-absorbing mechanisms.

overview of the conjugated carbon-based polymers and the microwave-absorbing mechanisms of their structures.

2.1 Carbon-based conductive polymers and their microwave-absorbing structures

Carbon-based microwave-absorbing materials (MAMs) have received attention in recent decades, from fundamental theoretical study to experimental design and analysis, due to the pursuit of this type of MAM for their excellent microwave-absorbing ability, and broad efficient bandwidth features, and lightweight and thin format (Zhao et al., 2016; Guan et al., 2021). Although conjugated carbonaceous materials with different morphologies have high dielectric losses, single dielectric loss shows inefficient bandwidth in electromagnetic absorption (EMA) owing to impedance mismatching. Metals, metal oxides, metal sulfides, elements, and other magnetic and dielectric materials have been anchored to the carbonaceous materials including carbon nanotubes (CNTs) (Munir, 2017; Peymanfar et al., 2019b; Peymanfar et al., 2019c; Mo et al., 2019; Chen et al., 2021a; Liu et al., 2021; Wang et al., 2022), carbon fibers (CFs) (Peymanfar and Moradi, 2020; Wang et al., 2020; Chen et al., 2021b; Chen et al., 2021c; Gunwant and Vedrtnam, 2021; Song et al., 2021; Wu et al., 2021), carbon spheres

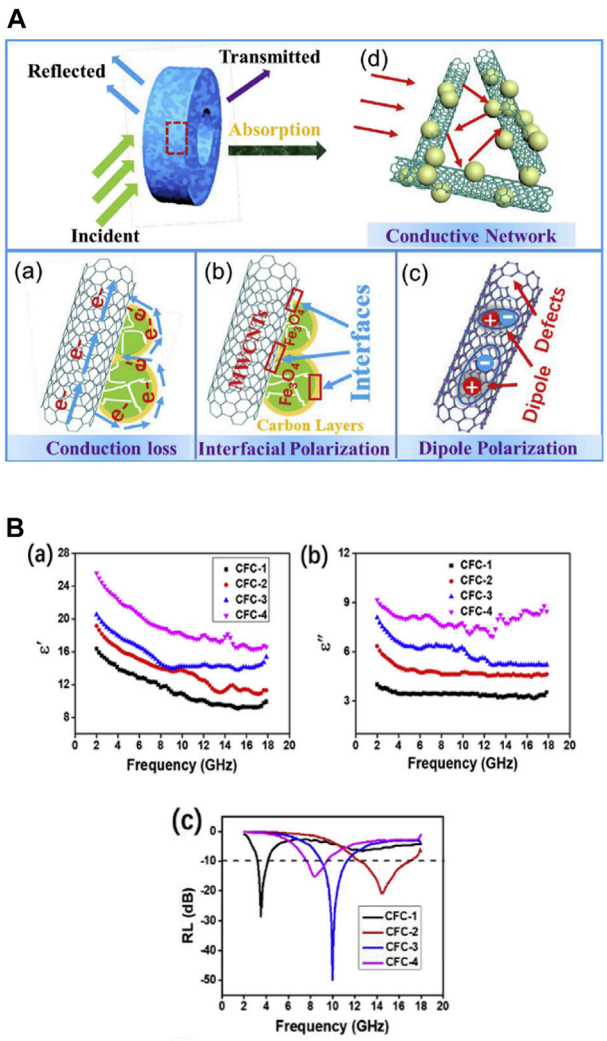

FIGURE 2
(Aa–d) Related microwave absorption mechanisms of C@Fe_2O_3@MWCNT composites, **(Ba)** real parts of the complex permittivity (ε′), **(Bb)** imaginary parts of the complex permittivity (ε″), and **(Bc)** the strongest absorption curve of the samples (Wang et al., 2019a).

(Ning et al., 2020a; Zhang et al., 2020a; Peymanfar et al., 2021a; Song et al., 2021), carbon micro-tubes (Peymanfar et al., 2021d), activated carbon (Mahmoodi et al., 2022), graphene (Li et al., 2017; Meng et al., 2018; Wang et al., 2019a; Peymanfar et al., 2019d; Zhi et al., 2021; Wu et al., 2022), carbon net-like morphology (Peymanfar and Ghorbanian-Gezaforodi, 2021), and carbon black (Ibrahim et al., 2020; Lalan and Ganesanpotti, 2020). This phenomenon can effectively enhance the microwave-absorbing ability of the conjugated structures due to the tunable electromagnetic properties and emergent synergetic loss mechanisms in the tailored composites (Duan et al., 2018; Chen et al., 2021b; Guan et al., 2021; Kumar et al., 2021).

In recent years, conjugated carbonaceous materials composited with different structures that provide outstanding microwave absorption have been reported. For instance, Che et al. architected a special conductive network with two types of carbonaceous structures with increased conductive and dielectric features. The ternary-phased C@Fe_2O_3@MWCNTs (CFC) showed diverse mechanisms consisting of the combination of relaxation and conductive losses, leading to thin, lightweight, and high-performance microwave absorbers. Figure 2A shows the possible microwave-absorbing mechanisms in the absorbing medium.

As shown in Figure 2Ba, higher MWCNT content causes more permittivity, suggesting a more conducive polarization loss mechanism.

Figure 2Bc shows a diagram of RL *versus* the frequency of microwave absorbers with diverse MWCNT ratios. The optimized absorber showed high-performance MA, with an RL of −49.9 dB at 2.0 mm in thickness. The multiphase component augmented the heterogeneous interfaces desirable for interfacial polarization (Wang et al., 2019a).

Wang et al. used two fascinating ternary structures, Ni@carbon nano-onions and Ni/carbon nanotubes anchored to graphene surfaces (Ni@C/G and Ni/CNT/G), tailored through an atomic layer deposition (ALD) NiO. Two different carbonaceous morphologies comprising carbon nano-onions and CNTs were grown on the surface of graphene using a chemical vapor deposition scenario. The unique morphologies provided the absorbers with multiple reflections and scattering, relaxation loss, natural and exchange resonance, eddy current loss, impedance matching, and conductive networks, which promoted microwave absorption. The results showed that the hybrid architectures demonstrated proper microwave-absorbing features with low filling ratios at low-frequency ranges compared to the related structures. The associated microwave-absorbing mechanisms are summarized in Figure 3A.

The ε′ and ε" of NCG with different Ni ratios are shown in Figures 3Ba, b. The imaginary and real parts of the permittivity are tunable by varying the Ni content. The permittivity curves essentially originated from the conductive loss and polarization. The complex permeability curves of NCG samples are shown in Figures 3Ca, b. The bumps are associated with natural and exchange resonances due to the presence of Ni. NCG 100 showed a maximum RL of −45.5 dB at 6.2 GHz with efficient bandwidth as wide as 5.6 GHz at a thickness of 2.5 mm. Figure 3D compares the RLs of the samples with diverse Ni contents, demonstrating the effect of Ni amount on microwave absorption (Xu et al., 2020).

Peymanfar et al. designed an interesting microwave-absorbing nanocomposite by wrinkling a nickel nanosheet and using it to cover grape-like carbon microspheres (CMSs). They also investigated the effects of the absorbing medium on the characteristics of microwave absorption. In the reported work, 2D Ni nanostructures were first prepared. Next, CMSs fabricated by the conventional hydrothermal method were decorated with the wrinkled nickel nanosheets using an ultrasonic and hydrothermal procedure. The special morphology obtained by wrinkled structure enhanced the polarization loss, boosting the microwave absorption. CMSs have a high surface area, low density, and proper dielectric properties owing to their conjugated structures. The effects of the combination of CMSs and Ni in PS and PVDF matrices showed improved electromagnetic absorption. Loading the CMSs diminished the matching thickness by modulating the complex permittivity and permeability, governed by the quarter wavelength mechanism. Compared to the sample fabricated by PS, PVDF showed increased impedance matching and

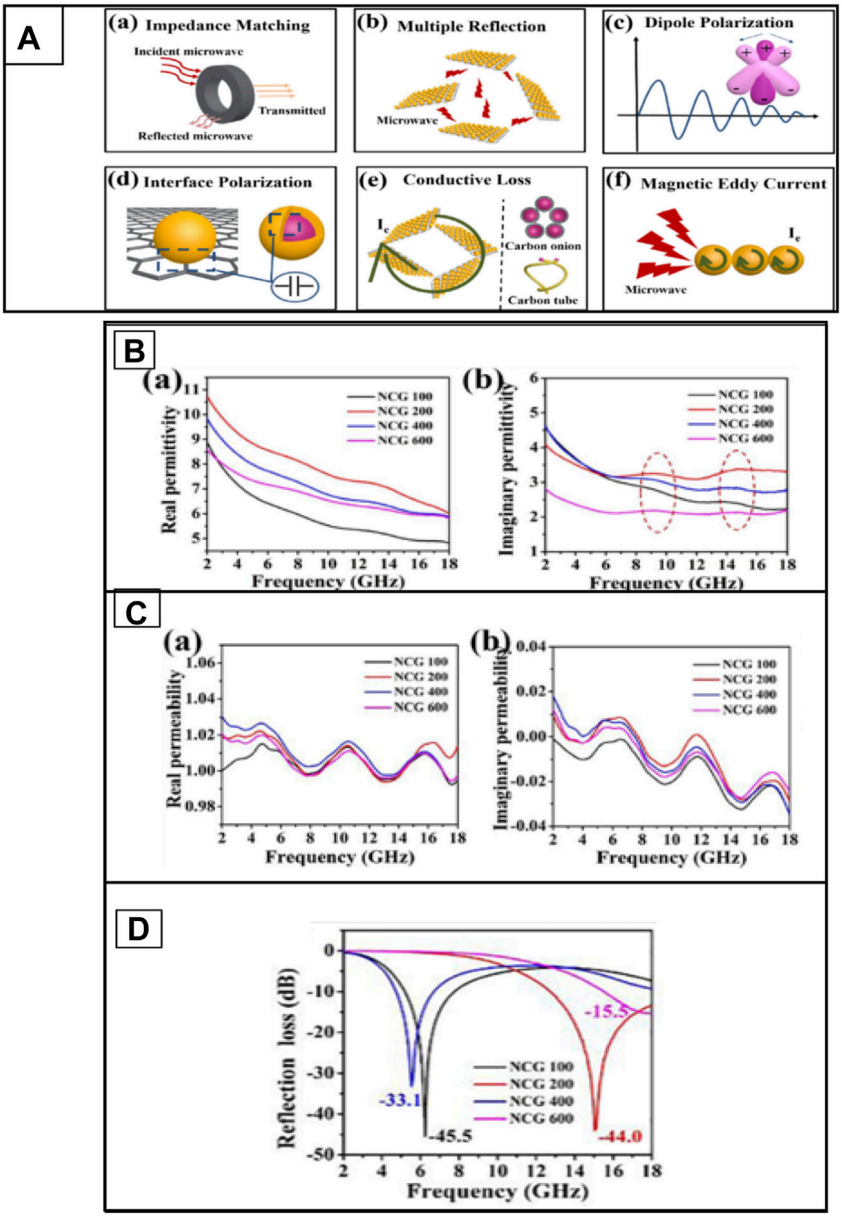

FIGURE 3
(A) Schematic illustration of the primary microwave-absorbing mechanisms in the Ni@C/G and Ni/CNT/G absorbers, **(Ba,b)** real and imaginary parts of the permittivity of the samples, **(Ca,b)** complex permeability *versus* frequency of NCG 100, NCG 200, NCG 400, and NCG 600, and **(D)** summarized RL results of the samples (Xu et al., 2020).

magnetic loss while reducing the relaxation loss. All the tailored samples exhibited narrow band gaps and substantial magnetic features. Notably, the results demonstrated that the architected microwave-absorbing and shielding structures showed considerable reflection loss, efficient bandwidth, and shielding properties with thin thickness owing to the wrinkled morphology of Ni and the applied media. Figure 4A showed the possible microwave-absorbing mechanisms in the absorbing matrix. As shown in Figure 4C, the Ni-containing composites exhibited diverse notches due to their natural and exchange resonances. Substitution of the PS by PVDF increased the imaginary part of the permeability but diminished both real and imaginary parts of the permittivity. The results also demonstrated that loading the CMSs generally boosted the real part of the permittivity compared to the Ni/PS nanocomposite. Moreover, the significant real part of the $Ni(OH)_2$/PS was established by dipole polarization and enhanced n $\rightarrow \pi^*$ transitions owing to the existing hydroxyl functional groups. Figure 4B shows the diagram of RL *versus* the frequency of microwave absorbers for the combination of different components. A comparison of the curves demonstrates the importance of carbon-based microspheres in ameliorating the microwave absorption. The maximum RL of the wrinkled Ni/PS was −50.53 dB at 11.52 GHz while that for the CMS/Ni/PVDF was −90.29 at 10.68 GHz (Peymanfar et al., 2021a; Lv et al., 2021).

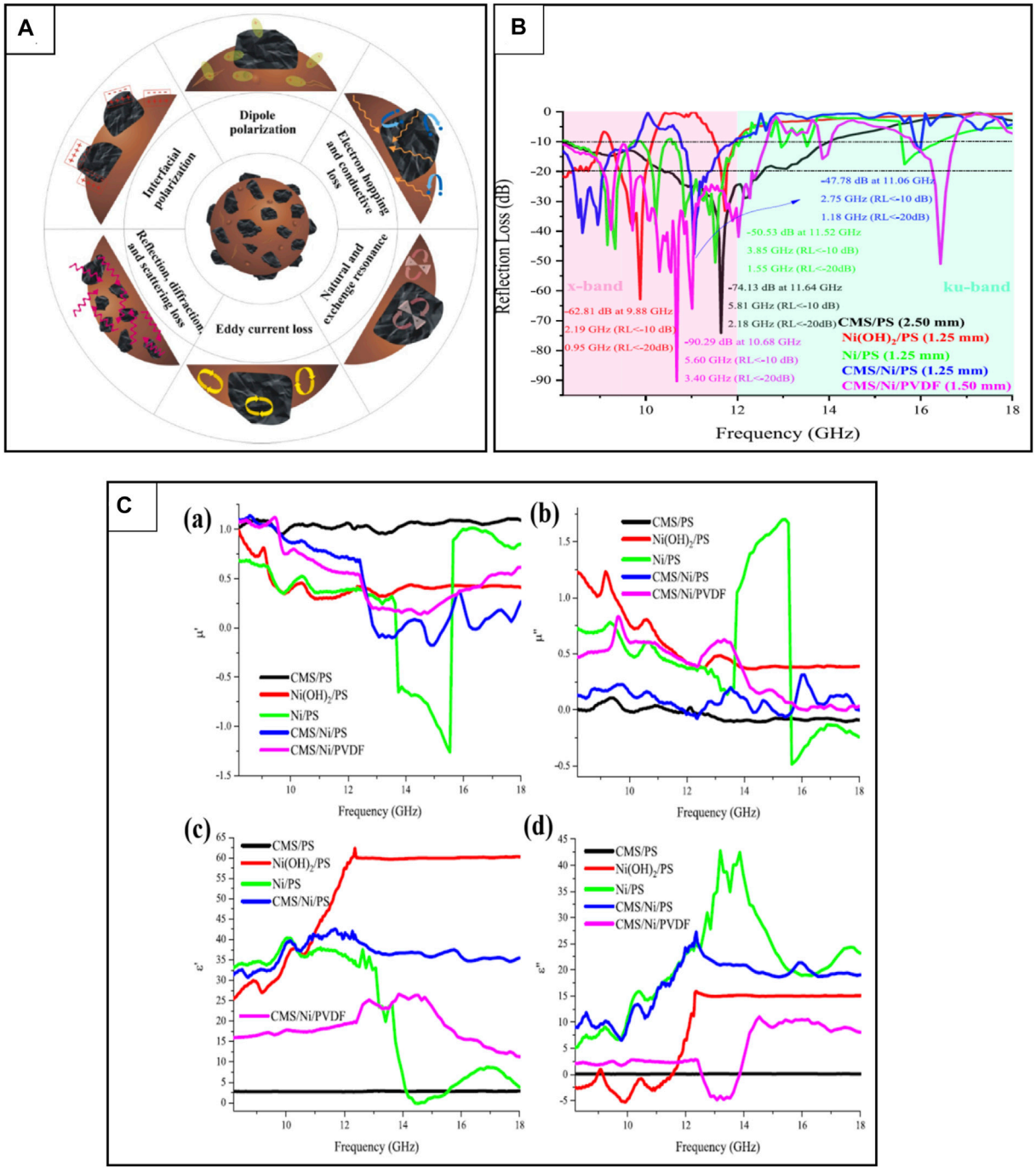

FIGURE 4
(A) Illustrative diagram of the microwave-absorbing mechanisms in CMC/Ni systems, **(B)** best RL values, **(Ca,b)** real and imaginary parts of permeability, and **(Cc,d)** real and imaginary parts of the permittivity of the samples (Peymanfar et al., 2021a).

Diao et al. (2021) were the first to design functional $Bi_2Te_{2.7}Se_{0.3}$/graphene foam (BTSGF) composites with thermoelectric materials $Bi_2Te_{2.7}Se_{0.3}$ (BTS) and GF showing satisfactory conductive and dielectric properties. In this structure, GF is the main component, with a conjugated backbone and high porosity that ameliorates the wave path, impedance matching, and RL. This material has intrinsic electromagnetic-absorbing properties due to its conjugated structure, resulting in conductive and relaxation losses as well as multiple reflections and scattering. To further improve the absorbing strength of the GF, the authors combined the BTS and graphene to form $Bi_2Te_{2.7}Se_{0.3}$/GF (BTSGF) composites through a solvothermal self-assembly method. The BTSGF composites showed enhanced microwave attenuation (MA) properties due to the various synergistic effects of BTS and GF, including conductive and polarization losses. More importantly, the BTS susceptibility to energy conversion is desirable for electromagnetic wave attenuation.

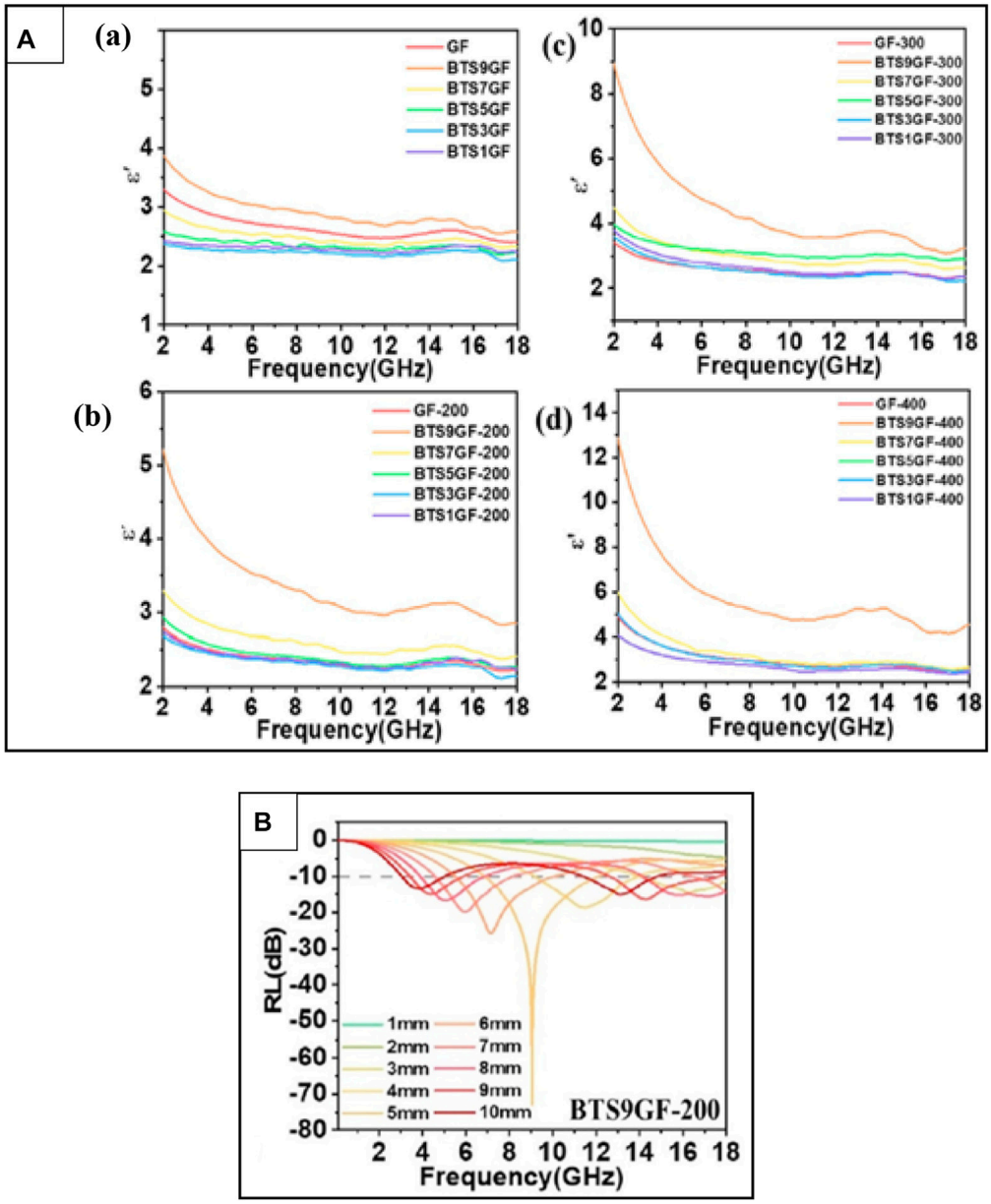

FIGURE 5
(Aa–d) Real and imaginary parts of the permittivity of the samples without additional annealing or at 200°C, 300°C, and 400°C annealing, respectively. **(B)** RL *versus* frequency curves of a selected sample with the best performance (Diao et al., 2021).

Therefore, the authors proposed a new electromagnetic wave thermo-electric loss MA mechanism, which is of great significance to the study of thermoelectric materials as high-efficiency MA materials.

Figure 5A shows the frequency dependence of the ε′ of BTSGF for different BTS loadings and annealing temperatures. As the calcination temperature increases, the ε′ of BTSGF with a lower BTS loading is basically unchanged, while the ε′ of BTSGF with a higher BTS loading (especially 90 wt%) increases significantly. The representative RL curves of BTS9GF-200 with different thicknesses are shown in Figure 5B. BTSGF with high BTS loading and annealing temperatures showed increasing thermoelectric properties and improved microwave absorption. Therefore, both the BTS loading and annealing temperature help to amplify the electromagnetic elimination of BTSGF. The optimized absorber showed high-performance MA properties with an RL of −73.0 dB at 5.0 mm in thickness (Diao et al., 2021).

Cao et al. (2015) (https://pubs.rsc.org/en/content/articlelanding/2015/tc/c5tc02185e/unauth) produced ultrathin graphene as a lightweight microwave absorber with high efficiency in thermally harsh environments by fabricating graphene oxide (GO) according to the modified Hummers' method and subsequent solution-based GO reduction. Graphene is a fascinating carbon-based material for microwave absorption

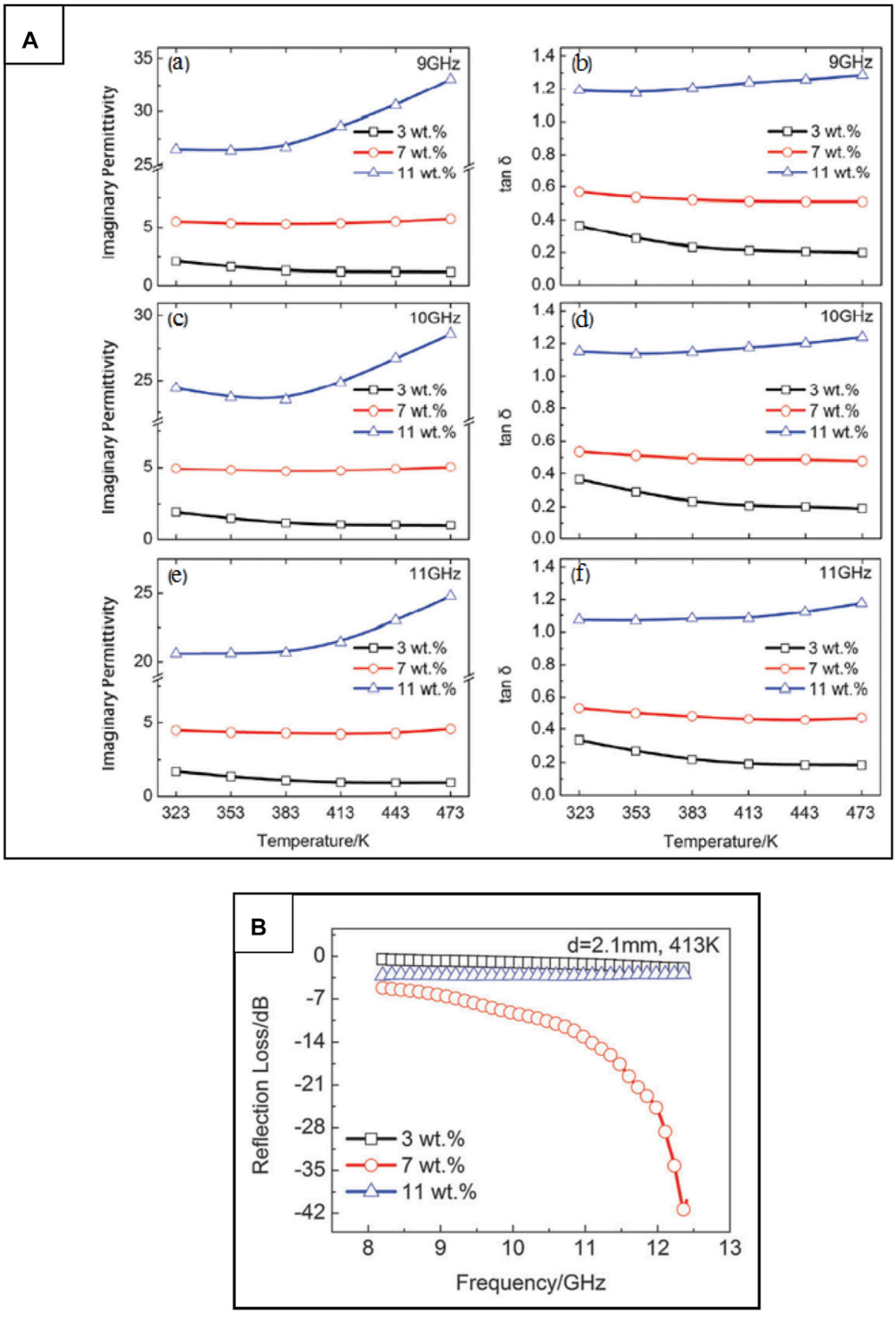

FIGURE 6
(Aa,c,e) Imaginary parts of the permittivity of the 3 wt%, 7 wt%, and 11 wt% composites *versus* temperature at different frequencies. **(Ab,d,f)** Loss tangents of the 3 wt%, 7 wt%, and 11 wt% composites *versus* temperature at different frequencies. **(B)** Strongest RL curve of the samples (Cao et al., 2015) (https://pubs.rsc.org/en/content/articlelanding/2015/tc/c5tc02185e/unauth).

owing to its lightweight structure; high specific surface area; notable charge carrier mobility; abundant defects; and numerous functional groups including hydroxyl, epoxy, and carboxyl groups, which increase relaxation loss. The composite exhibited different dependencies on changing temperature and concentrations toward imaginary permittivity and microwave absorption.

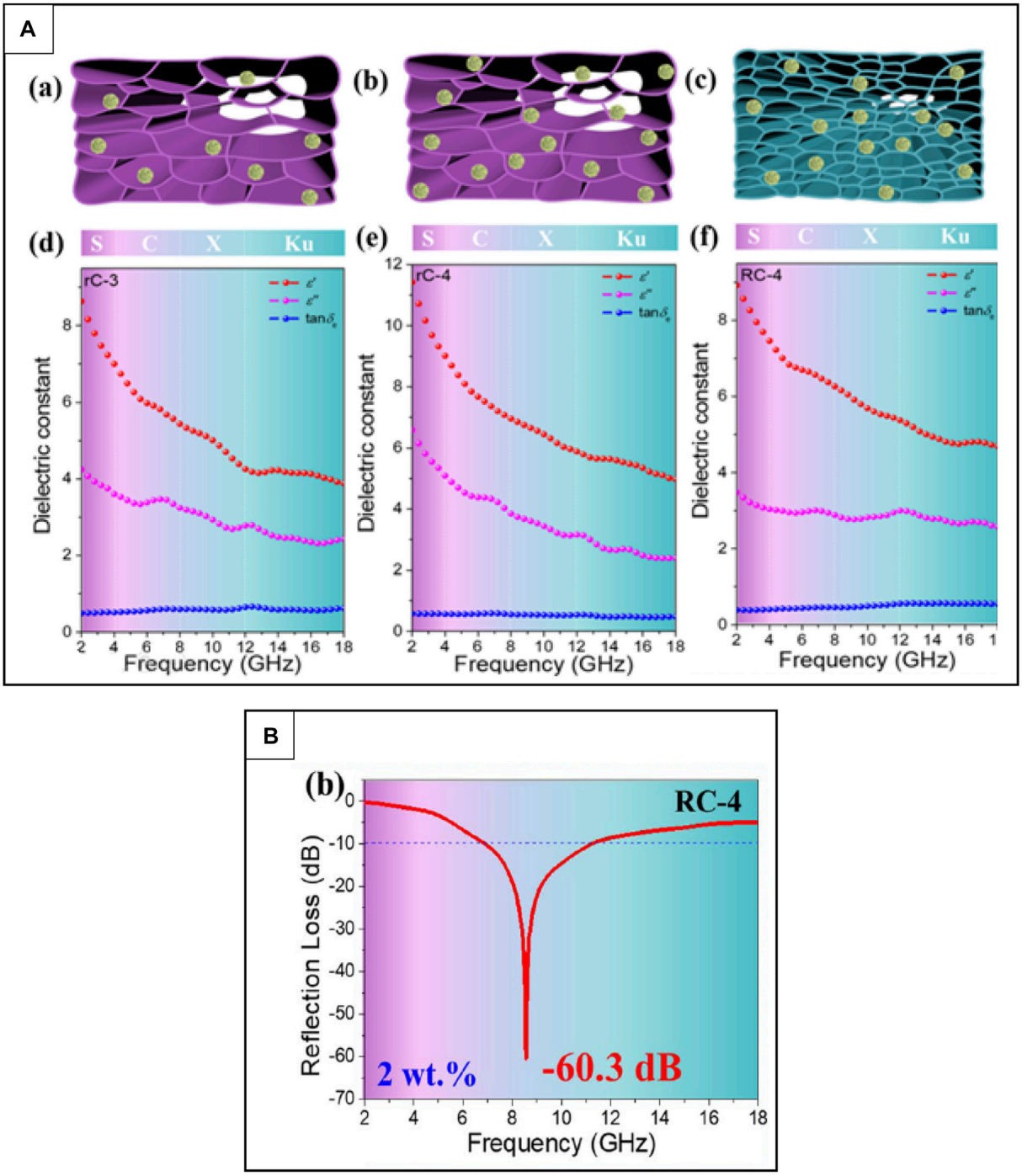

FIGURE 7
(Aa–c) Comparisons of the morphologies of the architected samples. **(Ad–f)** Dielectric constants of rC-3, rC-4, and RC-4. **(B)** RL results of the RC-4 sample (Wu et al., 2022).

Figure 6A shows the imaginary parts of permittivity *versus* temperature for different frequencies and ratios of graphene composites. The graph demonstrates that the conductivity and polarization tune the imaginary part of permittivity. The higher the graphene content, as the conjugated and conductive parts, the higher the permittivity, indicating more conductive and polarization losses. The imaginary permittivity of the graphene (3 wt%) composite was lower than others because the conductive network is not formed in the composite; thus, polarization loss is the main factor. Conductive networks form in the graphene (7 wt%) composite, augmenting the conductive loss. Therefore, a balance is formed between the increasing conductivity and decreasing polarization with increasing temperature; hence, the imaginary permittivity remains stable. In addition, the conductivity of the

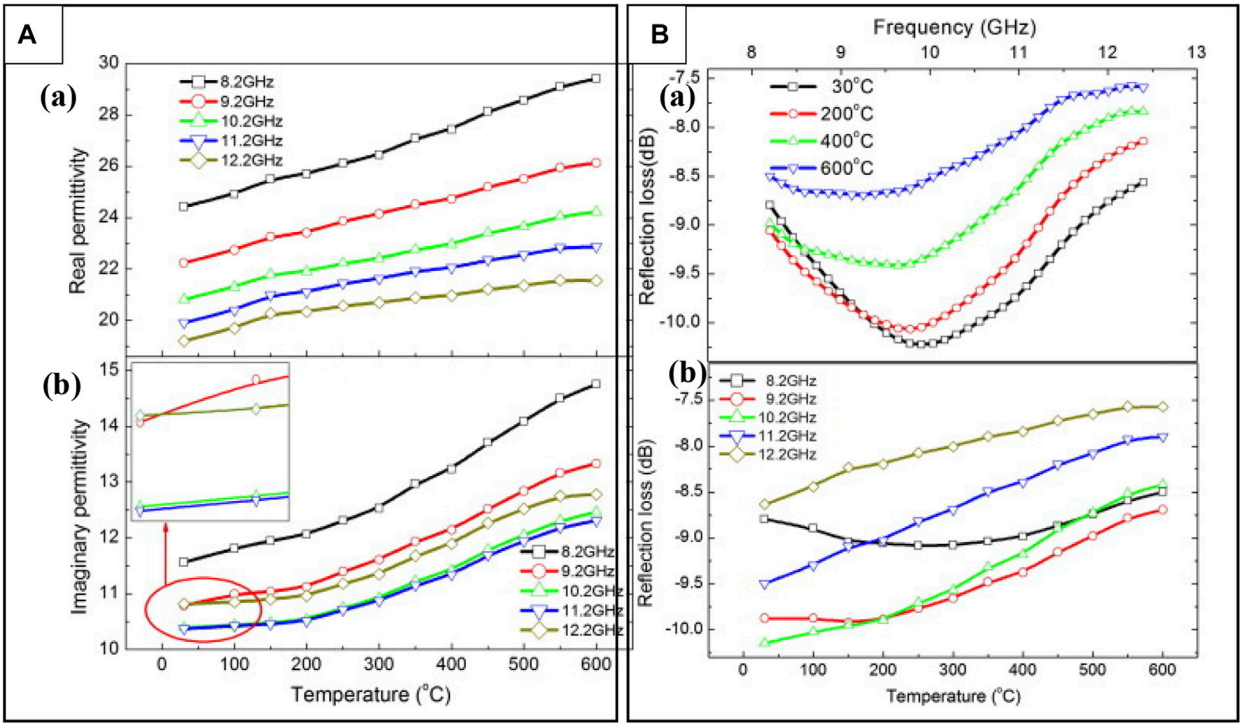

FIGURE 8
(Aa,b) Real and imaginary parts of the permittivity vs. temperature at various frequencies and **(Ba,b)** reflection loss vs. frequency and reflection loss vs. temperature related to the CF composite (Cao et al., 2010).

composite is higher in the 11 wt% composite, indicating that the imaginary permittivity increased with increasing temperature. Figure 6B demonstrates the reflection loss *versus* frequency for different graphene ratios. However, the expected result was better RL in the 11 wt% composite due to better dipole polarization and hopping conductivity; at some point, more GO will lead to more impedance mismatching and more reflection. Therefore, the 7 wt% composite showed better microwave-absorption properties compared to the 3 wt% and 11 wt% composites, showing the best RL of −42 dB with 2.1 mm thickness at 413 K. Accordingly, the fabricated ultrathin graphene composites showed highly efficient microwave absorption and thermal-stable permittivity at elevated temperatures.

Ji et al. designed a microwave absorber consisting of conjugated organic and inorganic sulfide materials to enhance MA performance and reduce IR emissivity. The authors modified the phase components (reduced GO (rGO) and CuS phases) and micro/nanostructure (microporous and nanosheet) by adjusting the amounts of CuS. Additionally, they changed the method of reduction (hydrothermal and ascorbic acid reduction), resulting in variations of pore structure and defects and modulation of the complex permittivity and microwave absorption. According to the structure of the composite aerogels, including rC-3 (hydrothermal reduction, 30 mg CuS), rC-4 (hydrothermal reduction, 60 mg CuS), and RC-4 (ascorbic acid reduction, 30 mg CuS), the EM parameters were further explored. As shown in Figures 7a–d, various CuS@rGO composite aerogel structures can be obtained by adjusting the amount of CuS and reduction methods. In addition, as illustrated in Figures 7d, e, f, rC−4 had the largest average dielectric complex permittivity, implying the stronger dielectric loss due to the higher CuS content in rC-4 compared to rC-3 due to more interfacial polarization. Furthermore, rC−4 formed more defects than RC-4 because the rGO in rC−4 was reduced at 120°C, compared to 95°C for RC-4. Moreover, rC−4 had a larger pore diameter than RC−4, which allowed higher attenuation of electromagnetic waves (EMWs). Although rC−4 showed excellent dielectric loss, RC-4 displayed excellent attenuation capacity (α) and impedance matching (Z) among the composite aerogels, with good absorbing performance. The superior efficiency may have occurred due to the higher number of functional groups and defects. As shown in Figure 7B, CuS@rGO composite aerogel obtained using ascorbic acid as a reductive agent showed an RL of −60.3 dB with a lower filler content (2 wt%) at a thickness of 3.5 mm. Thus, this work offered a facile method to design and develop porous rGO-based composite aerogel absorbers with radar-IR compatible stealth (Wu et al., 2022).

Cao et al. (2010) prepared a short carbon fiber/silica composite *via* conventional ceramic processing for practical applications in high-temperature microwave absorption. Carbon fibers (CFs) and their composites are attractive candidates as microwave absorbers due to their excellent electrical and mechanical properties for countless domestic and commercial applications. Moreover, their material properties can be predicted by calculating the reflection loss from the permittivity and permeability, which decreases the number of experiments required. The real part of the permittivity increases with increased temperature, which is ascribed to decreasing the

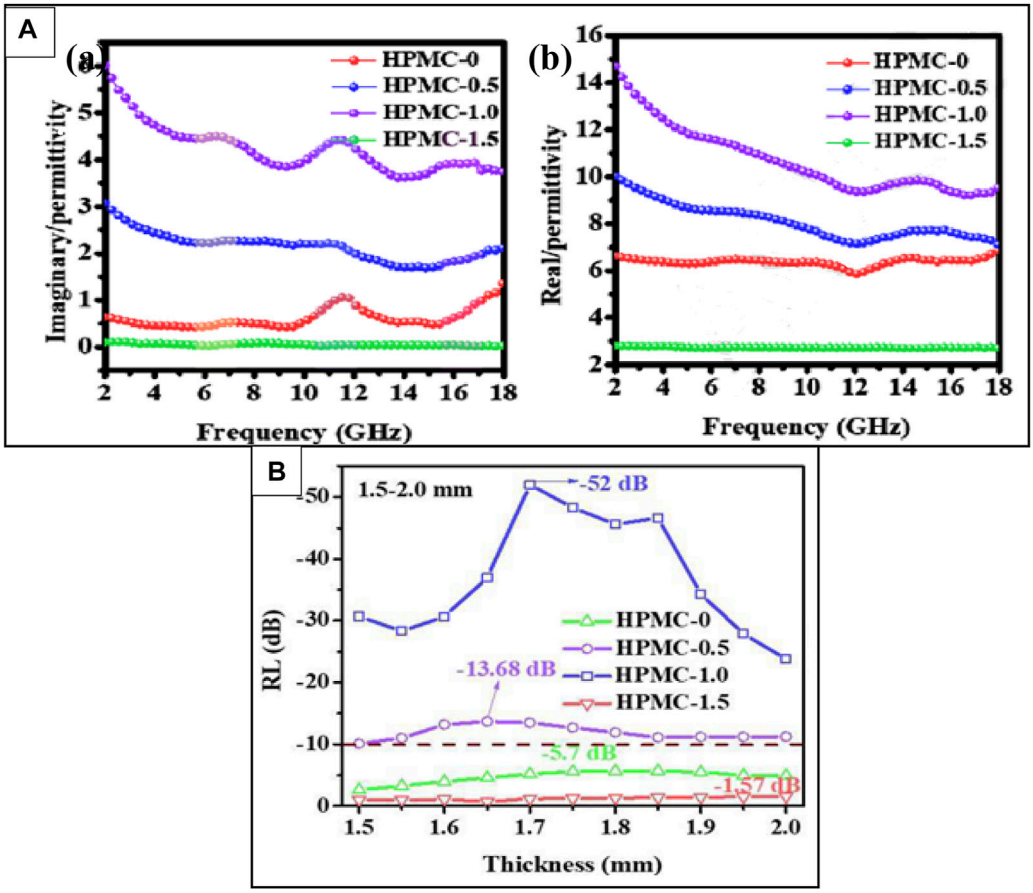

FIGURE 9
(Aa,b) Factors of permittivity and **(B)** RL values within 1.5–2.0 mm for all samples (Zhao et al., 2019).

relaxation time of electron polarization, and the imaginary part augments as well, which in this case originates from the enhanced electrical conductivity of the carbon fibers. Figures 8Aa, b, Ba, b show the RL dependence on temperature at various frequencies. The RL-temperature curves at five different frequencies imply a maximum CF/SiO_2 absorption peak around −10.22 dB at 9.90 GHz at 30°C, and −8.69 dB at 9.25 GHz at 600°C, indicating that the peak slightly shifts toward lower frequency with increasing temperature. These results showed that the microwave absorption of CF/SiO_2 at lower temperatures is greater than others at higher temperatures.

Zhao et al. (2019) fabricated a hierarchically porous magnetic carbon (HPMC) structure by introducing a magnetic substance on microstructure biomass material, which demonstrated excellent EMW performance. Biomass-derived materials provide novel microstructures, including heterostructures with unique morphology such as microtubular channels, which are challenging to produce by routine chemical synthesis (Peymanfar and Mirkhan, 2022). The authors used rice as an example of biomass materials and conducted pre-treatment by a simple dipping and sintering method to attain porous carbon with the benefits of Ni^{2+} incorporation as a magnetic resource. The regulation of the microstructure and composition of the samples was synchronously and simply achieved by modulating the ratio of KOH to rice treated with Ni^{2+} (NTR) powder. This work paved the path for the development of biomass materials as green, renewable, low-cost, and high-performance carbon-based microwave absorbers. Figure 9A, B shows the complex permittivity curves *versus* frequency for different KOH to NTR powder ratios. The HPMC-1.5 sample is composed of high-density metal Ni NPs; thus, it is reasonable that the low filler ratio of 15 wt% for HPMC-1.5 in the paraffin matrix results in low permittivity properties. Nevertheless, both the ε' and ε'' values of the other three specimens increase with increasing metal ratios. At low filler loading (15wt%), HPMC-1.0 showed better microwave absorption, which was mainly ascribed to the significant dielectric loss with polarization relaxation, conductive loss, multiple reflections, and synergistic magnetic loss. Figure 9B shows the remarkable RLs of HPMC-1.0 due to its fascinating hierarchical porous channels in nano/micron-scale, three-dimensional (3D) interconnected network, and favorable nickel content, which improved impedance matching. The sample showed a maximum RL of −52 dB at only 1.7 mm and wide efficient bandwidth of 5 GHz at a low filler content of 15 wt%.

2.2 Conjugated polymers with heteroatoms

Synthetic polymers such as polyesters and polyamides offer several advantages compared to natural polymers, including the easier synthesis of large quantities, non-significant batch-to-batch

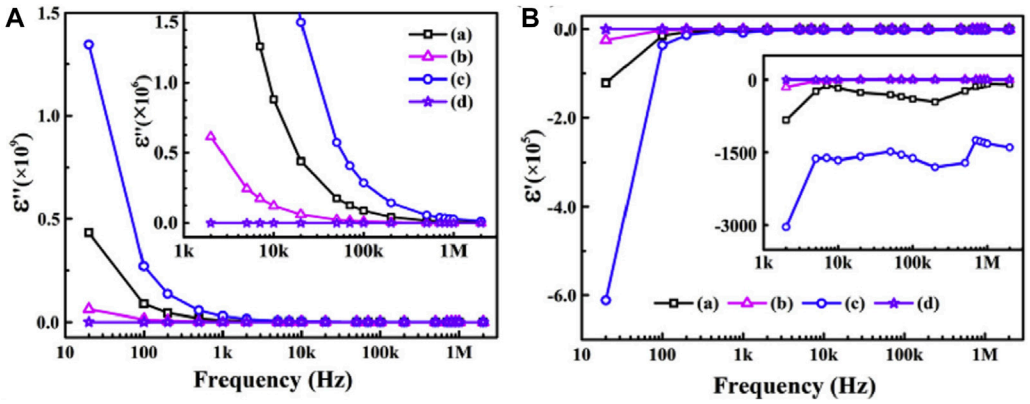

FIGURE 10
(A) Real part (ε′) and **(B)** imaginary part of permittivity (ε″) for four components [(a) CNS, (b) CNS-PDA, (c) CNS-PDA/Ag, and (d) CNSP] (Gu et al., 2019).

variations, and countless possibilities for modifications to achieve the desired properties (Maitz, 2015; Englert et al., 2018). As only the formulation parameters control the final properties of the materials, the chemistry of conductive polymers offers wide diversities of synthetic methods, allowing both the integration of conductive elements in different media and the construction of complex structures. This ability not only provides microwave-absorbing characteristics but also conforms to environmental constraints (Olmedo et al., 1993; Olmedo et al., 1995). These factors make polymers promising candidates to solve numerous problems in the microwave-absorbing field.

Gu et al. fabricated a metamaterial composite (metacomposite) in which carbon nanospheres (CNS) were discovered and supported on nanosilver-polydopamine (CNS-PDA/Ag). The impedance and optical band gap indicated that the CNS-PDA/Ag metacomposite broadened the conductive pathway to promote electrical conductivity. The remarkable point of this study was the high negative permittivity obtained from the merged secondary fields due to the unique structure of the hydrothermal and high-temperature annealing method.

As shown in Figures 10A, B, CNSP showed positive permittivity, while CNS showed negative permittivity. The explanation for this finding is the higher graphitization of CNS, which increases the electrical conductivity. By modifying the surface of CNS using PDA, the oxygen-containing functional groups were enriched, leading to a reduction in the electrical conductivity of CNS, regulating the conductivity in CNS-PDA. In CNS-PDA/Ag, the Ag nanoparticles are deposited on the surface of the CNS-PDA. Ornamenting the structure with PDA decreases the conductivity and expands the CNS-PDA structure. The negative permittivity in the CNS and CNS-PDA/Ag is caused by the increased electrical conductivity. The carbonization of CNSP and deposition of Ag nanoparticles facilitate charge circuits. The increased negative permittivity in CNS-PDA/Ag can be ascribed to the Maxwell–Wagner–Sillars effect. All three components—CNS, PDA, and Ag—expose anisotropy in dielectric properties and electrical conductivity, further impacting the electrical features of the final metacomposite (Gu et al., 2019; Lv et al., 2020).

In the last decade, polypyrrole (PPy) as a conjugated organic polymer with N as a heteroatom has gained attention as a microwave absorber (Peymanfar et al., 2018). Qi et al. fabricated a microwave absorber using conjugated conductive polymers. Conjugated microporous polymers (CMPs) are suggested due to their conjugate molecular fragments and permanent micropores. The process and precursors used to prepare the CPTPB, CPTPA, and CPTB are depicted in Figure 11A. The authors evaluated the permittivities of CPTPB (TB/pyrrole1:1), CPTPA (Tris (4-(PTPA)/pyrrole 1:3), and CPTB (PTB/pyrrole 1:3) with different ratios of pyrrole as a monomer. As shown in Figures 11Ca–f, CPTPB showed higher permittivity compared to that of pure PPy. Interestingly, the permittivity decreased with increasing amounts of pyrrole amount from CPTPB-3 to CPTPB-5, as shown by the reduced conductive and relaxation losses. Figures 11Ce, f confirm the increased permittivity by substituting CPTPB and CPTB with CPTPA. The synergic effect produced by the π-π stacking in the carbon-based conjugated structures was precisely dissected. This phenomenon tunes the heterogeneous interfaces, benefiting the interfacial polarization (Jiao et al., 2020).

To evaluate the effect of the doping agent ratio on the microwave-absorbing characteristics and energy band gap, Javanshir and coworkers used dodecylbenzenesulfonic acid (DBSA) as a doping agent to regulate polyaniline (PANi) features. The results showed that the amount of doping agent is a compromise with the energy band gap, DC electrical conductivity, and microwave absorption performance. Noticeably, polyacrylonitrile (PAN) was used as an absorbing medium instead of conventional paraffin wax. Paraffin has poor mechanical properties, which limit its practical applications. PAN can be used as a polymeric matrix in two ways: first, the useful mechanical features of PAN promote its practical applications. Second, the presence of nitrile functional groups allows the $n\rightarrow\sigma^*$, $n\rightarrow\pi^*$, and $\pi\rightarrow\pi^*$ transitions to augment the polarization, relaxation loss, electron hopping, micro currents, and conductive networks desirable for microwave attenuation. Figure 12Aa–d shows the dependence of frequency on the complex permittivity of the sample. The regulation of the molar ratio between aniline and DBSA (Aniline: DBSA = 10.0, 7.5,5.0.2.5, denoted as PANi10.0,

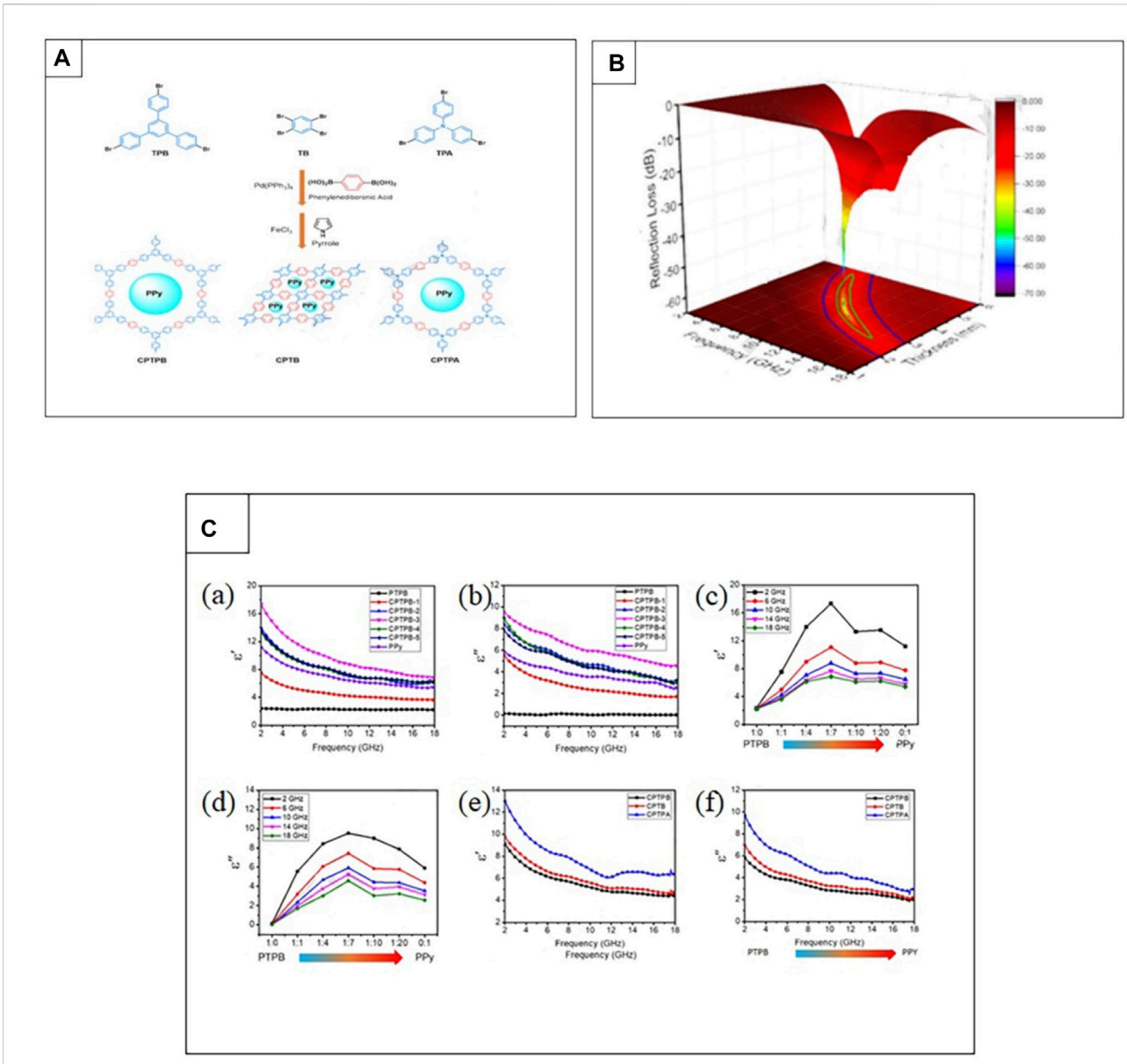

FIGURE 11
(A) Synthetic procedure for conductive CMPs, **(B)** RL value of the CMPs, and **(Ca–f)** real (ε′) and imaginary parts of permittivity (ε″) of the structures prepared in the diverse routes (Jiao et al., 2020).

7.5, 5.0, and 2.5) modifies the morphology and microwave-absorbing ability of the tailored conjugated polymers. The microwave-absorbing features affect the specific surface area, modulating polarization loss and conductive capacity, which are adjusted by oxidative doping. The results showed that the amount of oxidative dopant regulates the energy bandgap, influencing the relaxation loss. Figure 12B presents the microwave absorption performance of the samples with different molar fractions of the doping agent. The specific mechanisms originating from the architected morphologies and chemical structures led to the metamaterial features and permeability of the samples, promoting impedance matching and microwave-absorbing properties (Peymanfar et al., 2021b; Yang et al., 2022b) (https://www.sciencedirect.com/science/article/abs/pii/S0032386120308065).

Researchers have also assessed 2D nanomaterials. Carbon nanotubes and carbon-based structures (exclusively graphene and g-C_3N_4) have attracted attention due to their high degrees of microwave absorption (Peymanfar and Ghorbanian-Gezaforodi, 2020; Peymanfar et al., 2021e). Mohammadi et al. fabricated g-C_3N_4/polythiophene (PTh) composites utilizing various mass fractions of conjugated structures, resulting in efficient bandwidths for all samples. This occurred for polarization and conductive losses, which was promoted by $\pi \rightarrow \pi^*$ and $n \rightarrow \pi^*$ interactions between the PTh and nanosheets, as well as the metamaterial features in the composites, which provided permeability in the microwave absorbers and improved impedance matching and microwave attenuation. As shown in

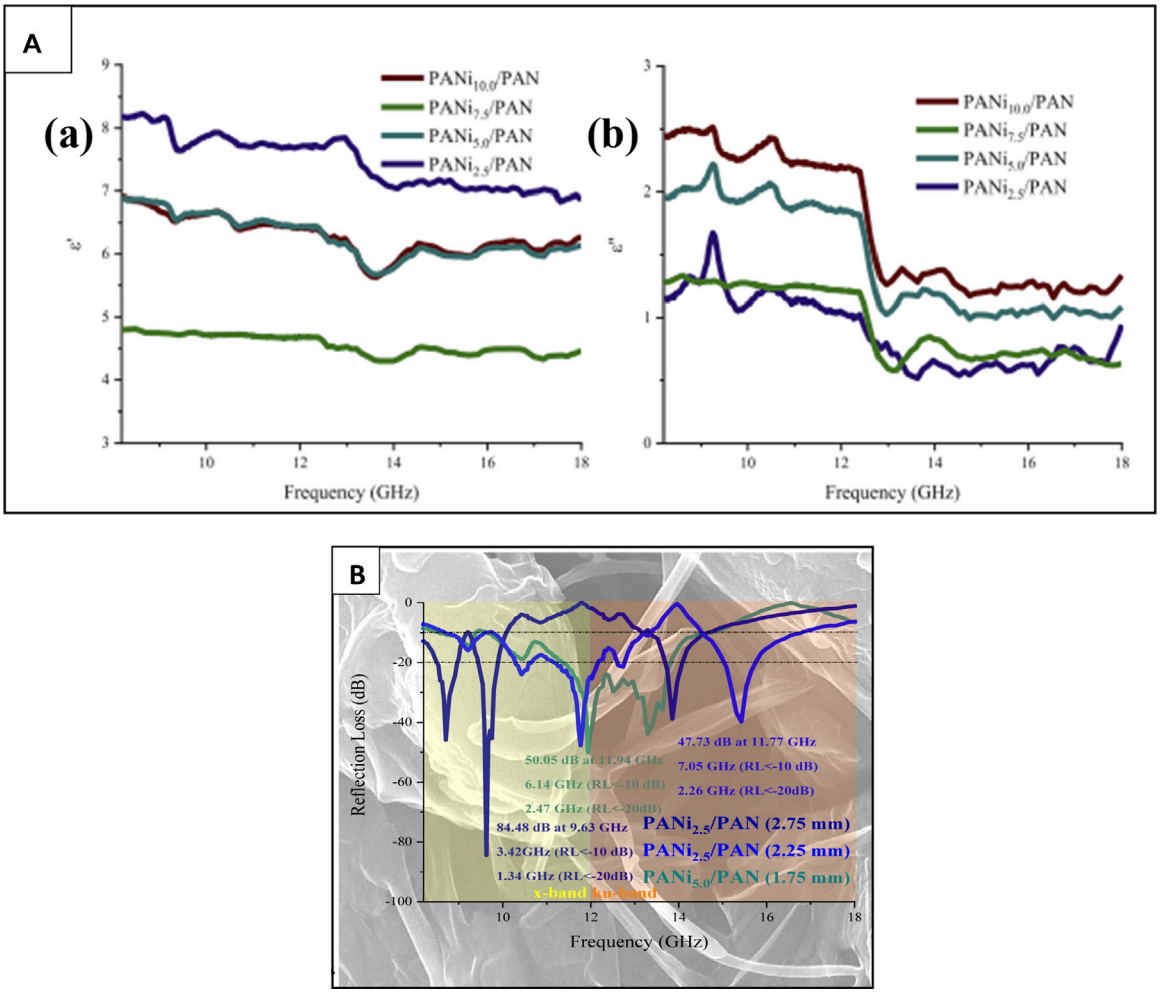

FIGURE 12
(Aa,b) Relative complex permittivity of the samples and **(B)** microwave absorption of the manipulated PANi from 8.2 to 18 GHz (Peymanfar et al., 2021b) (https://www.sciencedirect.com/science/article/abs/pii/S0032386120308065).

Figure 13Aa–d the real and imaginary parts of permittivity in the g-C_3N_4/PTh (30%)/PS increased due to interactions between the 2D structures and PTh, boosting the dielectric characteristics. The charge transition between the conjugated structures establishes conductive networks leading to the negative part of permeability of the g-C_3N_4/PTh (70%)/PS. Figure 13B shows the graph of RL *versus* the frequency of g-C_3N_4/PTh (30%)/polystyrene (PS). PS was used as an absorbing matrix, which has practical applications for the final product due to its mechanical features and the regulation of microwave absorption owing to its chemical structure (Peymanfar et al., 2020a).

Chang and co-workers designed a Fe_3O_4/polypyrrole/carbon nanotube ternary composite in which Fe_3O_4 nanoparticles were synthesized by a hydrothermal method at different sizes (H-Fe_3O_4, 100 nm (and (C- Fe_3O_4, 20 nm). First, the Fe_3O_4/PPy composite was prepared; CNTs were then added to the final composition as a reinforcer. In this composite, PPy and CNT increased the permittivity with the dielectric properties. In addition, the amount of PPy directly affected the RL. The results showed that when PPy is composited with Fe_3O_4, the magnetic properties of Fe_3O_4 and the permeability decreased. Furthermore, increasing the amount of CNT showed no significant change in μ' and μ'', suggesting that Fe_3O_4 nanoparticles played a crucial role in complex permeability. The value of ε' was less than the value of ε'' and the HPC series composite showed the highest ε' and ε'' values. The results indicated that with increasing PPy, ε'' increased; however, the presence of polypyrrole without magnetic material was not efficient and the combination was required to improve ε' and ε'' and, ultimately, microwave absorption. Figure 14Aa–c shows that, among the samples, the HP3C composite with 20% CNT showed the best absorption, with an RL of −25.9 dB at 2.0 mm in thickness (Yang et al., 2016).

Zhang et al. reported a conductive network constructed by a binary core-shell PPy/Fe3O4 composite prepared by chemical oxidative polymerization with polyvinyl alcohol and p-toluenesulfonic acid. The dielectric properties of PPy and the magnetic loss of iron affected the absorption parameters; thus, the

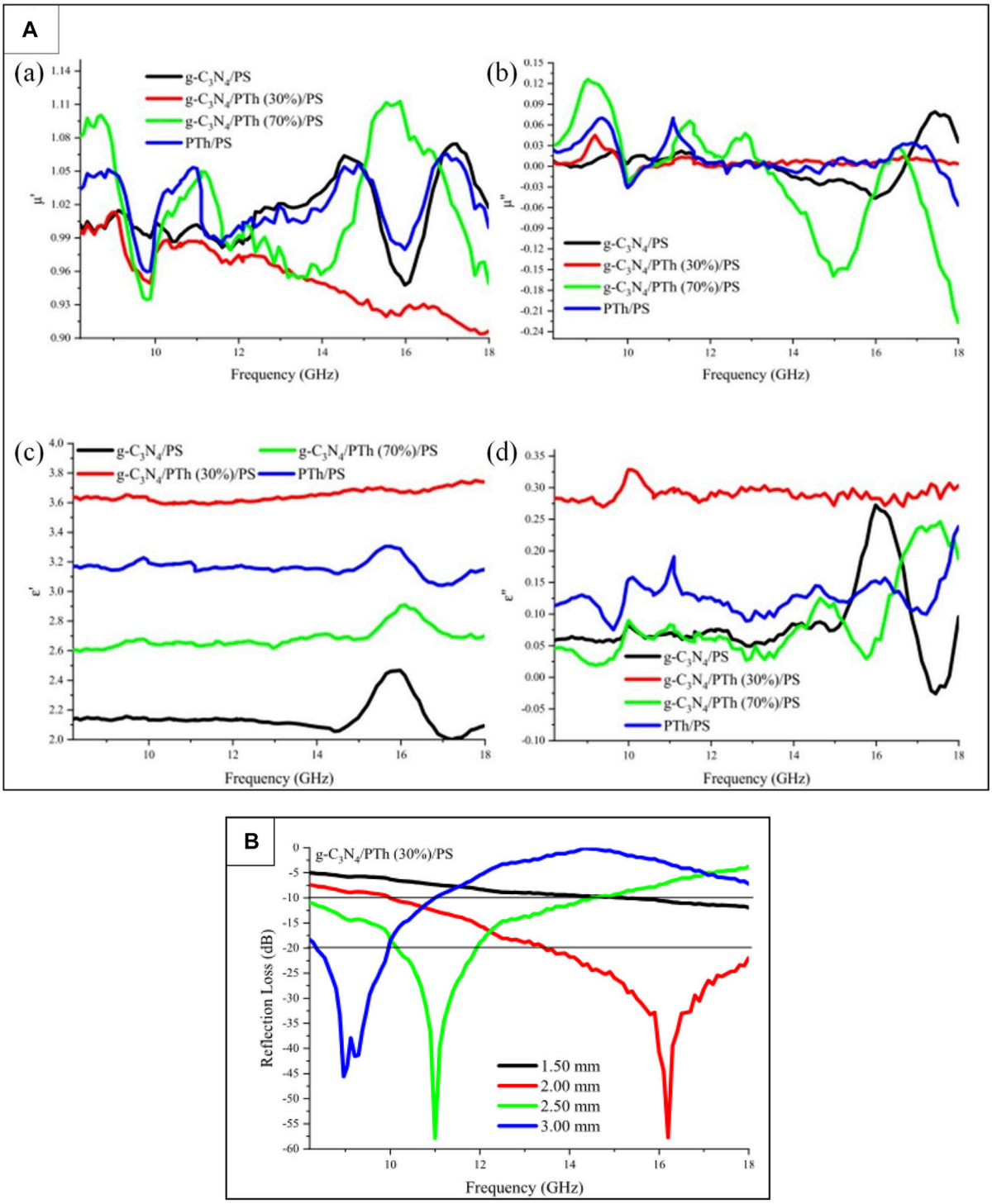

FIGURE 13
(Aa–d) μ′ and μ″ and ε′ and ε″ of the samples along the x and ku-band and **(B)** microwave absorption of g-C_3N_4/PTh (30%)/PS in 8.2–18 GHz (Peymanfar et al., 2020a).

combination of these materials created efficient microwave absorption. The diameter of the PPy shell varied from 20 to 80 nm to regulate the microwave absorption properties. Important points in the preparation of PPy/Fe_3O_4 composites are physical and chemical approaches. The preparation of PPy/Fe_3O_4 composites by chemical method demonstrated better RL performance from the broadened interfaces. Figure 15 shows that by increasing the mass fraction of PPy, ε' and ε'' are enhanced because PPy increases the conductive loss due to the presence of conjugated bonds and dielectric properties; however, μ' and $\mu''$are

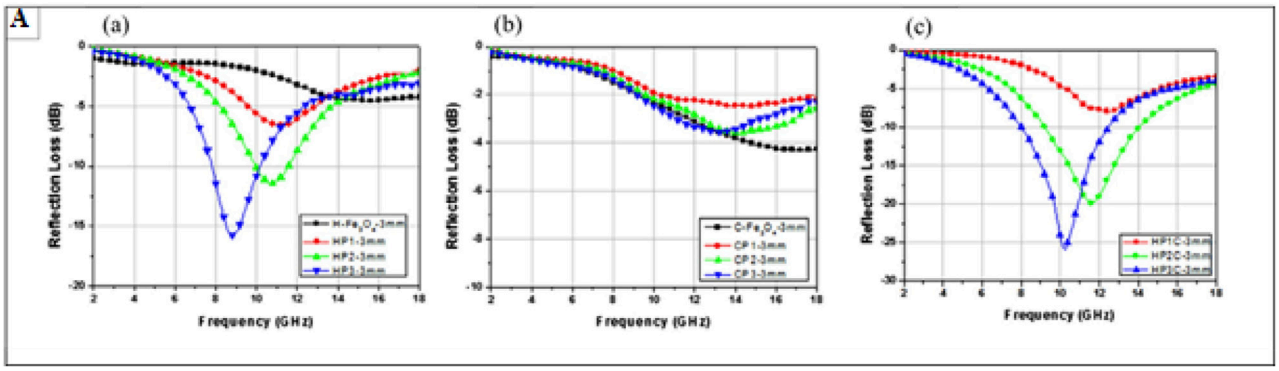

FIGURE 14
(Aa–c) RL values of samples 2.0 mm in thickness (Yang et al., 2016).

decreased due to the reduction of magnetic filler. Figure 15 shows the best RL of -31.5 dB (15.42 GHz) at 2.5 mm thickness for a PPy shell thickness in pyrrole@Fe3O4 composites of 80 nm (Qiao et al., 2016).

The magnetic shortcomings leading to the impedance mismatching of the conjugated polymers as dielectric structures can be addressed by inserting magnetic structures. Moreover, the polarization mechanisms and impedance matching can be tuned by loading other dielectric materials. Table 1 shows some binary and ternary composites designed to mitigate the EMWs.

3 Mechanisms allowing microwave absorption in conductive polymer structures

The prominent mechanisms that allow microwave attenuation of conjugated carbon-based materials can be summarized as conductive and polarization losses (Pattanayak et al., 2021; Huynen, 2022). The morphology is the essential factor in tuning the polarization loss characteristics (Peymanfar et al., 2021c). Moreover, the presence of heteroatoms and defects in the chemical structure of the conjugated backbone generates dipole polarization. Overall, polarization loss is governed by Debye relaxation and the Maxwell–Wagner model. The charge transitions from π to π^* and n to π^* are the vital parameters for conductive loss in organic conductive polymers. Meanwhile, inserting hetero atoms and negative/positive doping these types of materials changes the gap between the highest occupied molecular orbital (HOMO) and the lowest unoccupied molecular orbital (LUMO), thus affecting orbital orientations, rearranging the orbital occupation by charges, and influencing the conductive and polarization losses. Hence, the conductive and polarization losses of organic conductive polymers are tunable by 1) oxidative, reductive, and elemental doping; 2) etching to establish defects; and 3) modifying the synthetic scenarios to regulate the morphology and conjugated lengths. The missing permeability can be supplied by inserting magnetic structures or creating secondary fields, as discussed in the following sections. Table 2 shows the essential parameters in the microwave absorption field established by organic conductive polymers, leading to the RL. The RL was evaluated based on the transmission line theory equation (Eq. 1). The critical parameters in microwave absorption are permeability, permittivity, and impedance matching (Z, Eq. 2) (Zhou et al., 2022a). The essential factors modulating permittivity in conjugated polymers are electrical conductivity (conductive loss, Eq. 3) and polarization, listed to interfacial polarization and dipole polarization in the microwave region which is deduced by the Debye relaxation theory (Eq. 4). In contrast, natural and exchange resonance, as well as eddy currents, regulate permeability (Eqs 5 and 6) (Yang et al., 2022a; Zhou et al., 2022b; Zhou et al., 2022c). Accordingly, higher saturation magnetization and lower anisotropy increase magnetic loss. Particularly, the more constant the eddy current curve, the higher the eddy current loss. In organic polymers used as microwave-absorbing structures, the facile transition electrons between the conjugated structures amplify the permittivity of the conductive polymer. Thus, both polymer chain length and the use of heteroatoms as doping agents tune the RL. The morphology modification by changing the heterogeneous interfaces is a pivotal factor regulating the polarization loss and permittivity of microwave absorbers (Zhou et al., 2022a; Yang et al., 2022b). The wave entering from the absorber threshold can be canceled by the reflected waves from the reflector, on which the absorbing medium is placed when the input and reflected waves are 180° out of phase and the matrix thickness is the odd numeral of λ/4 of propagated wave (Eq. 7). The attenuation constant (α, Eq. 8) is the vital factor clarifying the absorber capacity to energy conversion. A trade-off exists between the attenuation constant and impedance matching to achieve a high RL (Peymanfar et al., 2020a; Zhang et al., 2021c). Table 3 has summarized the definitions of the symbols used to assay the microwave-absorbing characteristics.

The charge transitions in conjugated structures establish electrical conductivity and polarization mechanisms. The polarized structures can act as quasi-antenna and the charge circuits can develop secondary fields, creating metamaterial property and permeability to improve impedance matching. The possible mechanisms are illustrated in Figure 1. In the next section,

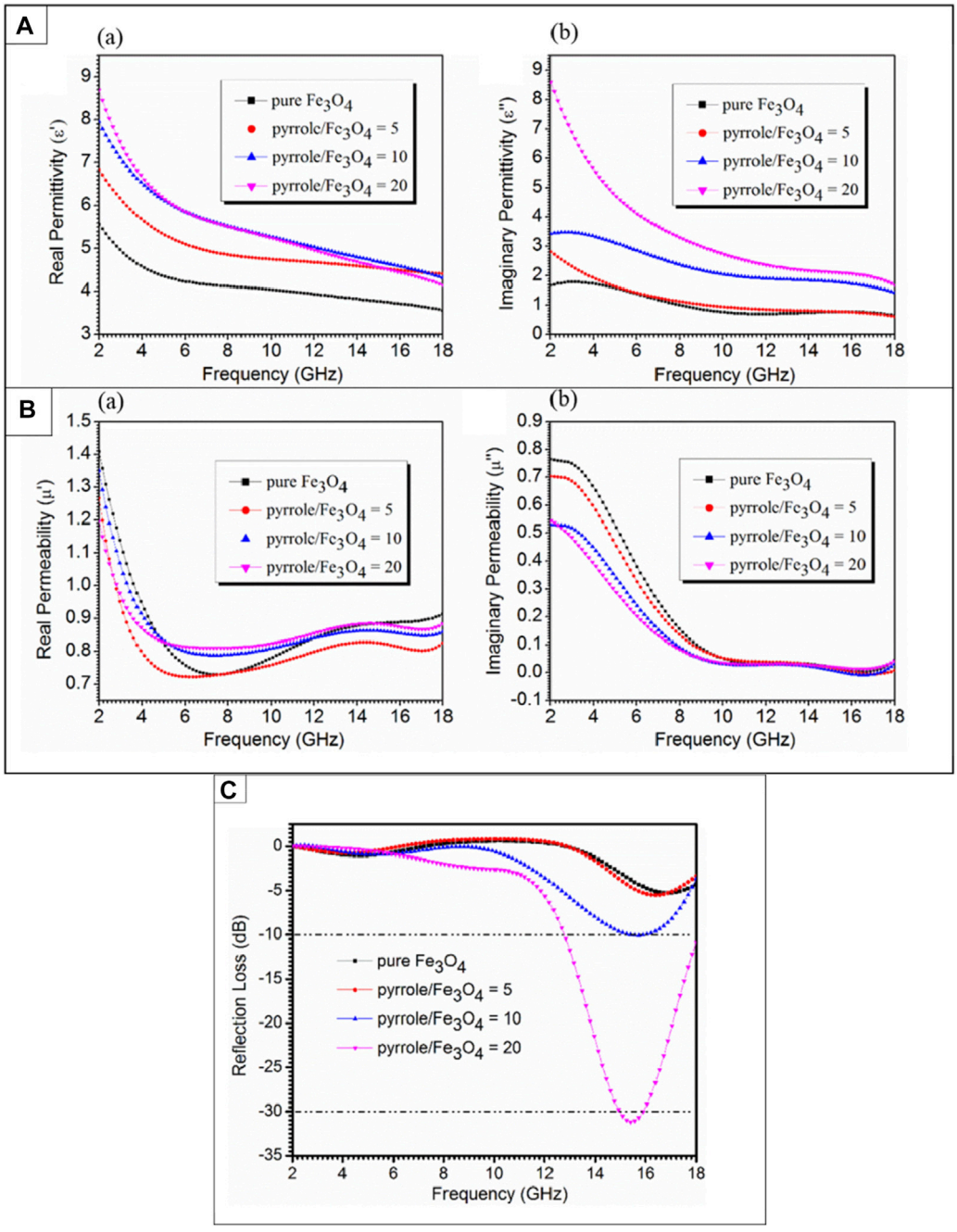

FIGURE 15
(Aa,b) Real and imaginary parts of permittivity, **(Ba,b)** real and imaginary parts of permeability, and **(C)** microwave absorption of PPy/Fe3O4 at 8.2–18 GHz (Qiao et al., 2016).

the metamaterial characteristics and quasi-antenna are promising mechanisms paving a new path in architecting conjugated carbon-based microwave-absorbing materials.

3.1 Metamaterials

Meta-materials (MTMs) are the new generation of artificially manufactured materials that are not found in the natural environment (Jia et al., 2018). In recent years, MTMs have been the subject of extensive studies to enhance and improve their characteristics and applications (Zhang et al., 2020c). MTMs are important due to their unusual electromagnetic properties including backward propagation, negative refraction index, reverse Doppler effect, negative permeability, negative permittivity, and perfect absorber action (Chen et al., 2006; Zhou et al., 2009; Qin and Brosseau, 2012; Song et al., 2013; Cheng et al., 2017a). Instead of relying on their combination, the exotic electromagnetic

TABLE 1 Microwave absorption performance of organic conductive polymer composites.

Absorber (binary or ternary)	Max. RL (dB)- matching frequency (GHz)	Matching thickness (mm)	Efficient bandwidth RL < −10 dB (GHz)	Reference
Ni@Co/C@PPy	−48.8-5.1	2.0	5.1	Bi et al. (2022)
TiO_2@Fe_3O_4@PPy	−61.8 - 8.7	3.2	6.0	Ding et al. (2019)
Fe_3O_4/PPy/CNT	−25.9-10.2	3.0	4.5	Yang et al. (2016)
$SrAl_{1-3}Fe_{10-7}O_{19}$/MWCNT/PANi	−24.9 -16.4	6.5	2.8	Peymanfar et al. (2019c)
CC/PANi aerogel	−54.8~14.0	2.1	5.1	Zhang et al. (2020b)
FeCoNi/PANi/PPy	−16.0- 14.2	2.5	2.7	Atassi and Fun (2020)
Porous carbon/PANi	−72.2~12.5	2.6	6.6	Zhang et al. (2021b)
FeCo@carbon nanoparticles encapsulated in polydopamine	−67.8 -15.8	2.0	5.3	Wang et al. (2019b)
C@Fe_2O_3@MWCNTs	−49.9 -10.0	2.0	≈2.0	Wang et al. (2019a)
Fe_3O_4@PPy	−31.5 -15.5	2.5	5.2	Qiao et al. (2016)
PPy@PANi	−34.8-13.9	2.0	4.7	Tian et al. (2015)
PPy nanofibers/Fe_3O_4	−41.6~13.0	2.5	≈4.0	Zhan et al. (2019)
PPy/Co	−20.0-13.8	3.0	7.2	Luo and Gao (2014)
$CoFe_2O_4$/carbon sheets/PANi	−51.8-12.4	2.6	7.2	Hou et al. (2021)

TABLE 2 Equations used to examine the electromagnetic wave-absorbing performance.

Eq.	Title	Formula
1	Transmission line theory	$R\,(dB) = 20\,Log\lvert\frac{Z_{in}-Z_0}{Z_{in}+Z_0}\rvert$, $Z_{in} = \sqrt{\frac{\mu_r}{\varepsilon_r}}\tanh[j\sqrt{\mu_r\varepsilon_r}\,f\,(\frac{2\pi}{c})d]Z_0$, $Z_0 = \sqrt{\frac{\mu_0}{\varepsilon_0}}$, $\varepsilon_r = \varepsilon' - j\varepsilon''$, and $\mu_r = \mu' - j\mu''$
2	Impedance matching	$Z = \frac{Z_{in}}{Z_0} = \sqrt{\frac{\mu_r}{\varepsilon_r}}$
3	Free electron theory	$\sigma_{AC} = \varepsilon''\omega\varepsilon_0$, $\varepsilon_0 = 8.854{*}10^{-12}Fm^{-1}$, and $\omega = 2\pi F$
4	Debye relaxation theory	$(\varepsilon' - \frac{\varepsilon_s+\varepsilon_\infty}{2})^2 + (\varepsilon'')^2 = (\frac{\varepsilon_s-\varepsilon_\infty}{2})^2$
5	Magnetic loss equations	$\mu' = 1 + \frac{M}{H}\cos\theta$, $\mu'' = 1 + \frac{M}{H}\sin\theta$, and $\mu_i = \frac{M_s^2}{akH_cM_s+b\lambda\xi}$
6	Eddy current loss	$C_0 = \mu''(\mu')^{-2}f^{-1}$
7	Quarter wavelength mechanism	$t_m = \frac{nc}{4f_m\sqrt{\lvert\varepsilon_r\rvert\lvert\mu_r\rvert}}$
8	Attenuation constant	$\alpha = \sqrt{\sqrt{(\varepsilon_r''\mu_r'' - \varepsilon_r'\mu_r')^2 + (\varepsilon_r'\mu_r'' + \varepsilon_r''\mu_r')^2} + (\varepsilon_r''\mu_r'' - \varepsilon_r'\mu_r')}\ \frac{\sqrt{2}f\pi}{c}$

characteristics depend on the sub-wavelength geometry of periodic resonance structures (Xin et al., 2017). Due to the unique properties of MTMs, they have been employed in vast and various fields such as filters (Sabah and Uckun, 2009), electromagnetic cloakings (Cummer et al., 2006; Schurig et al., 2006; Rajput and Srivastava, 2014; Colombi et al., 2015), super-lenses (Aydin et al., 2007; Amireddy et al., 2016), radars (Kurihara et al., 2005), antennas (Enoch et al., 2002; Alici and Özbay, 2007), solar cells (Hao et al., 2010; Bian et al., 2013), concealments (Tak et al., 2016), reduction of automotive false imaging, and microwave absorbers (Xin et al., 2017).

Landy et al. (2008) were the first to introduce the perfect metamaterial absorber (MMA) consisting of split-ring resonance structures with a middle dielectric layer. Generally, MMAs include three layers: a dielectric spacer, metallic structures, and a metallic mirror, which can be used to form MMAs with various designs (Duan et al.,

TABLE 3 Definitions of the symbols used to evaluate the microwave-absorbing features.

Symbol	Definition	Symbol	Definition	Symbol	Definition
ε'	Real part of permittivity	ε''	Imaginary part of permittivity	ε_0	Permittivity constant
μ'	Real part of permeability	μ''	Imaginary part of permeability	μ_0	Permeability constant
ξ	Elastic strain parameter	λ	Magnetostrictive coefficient	H_c	Coercivity
d	Thickness of absorber	c	Velocity of light in free space	Z_{in}	Input impedance
θ	Phase lag angle	*a*	Composition constant	*k*	Proportional coefficient
Z_0	Free-space impedance	f	Frequency	n	Odd number
ε_r	Relative complex permittivity	μ_r	Relative complex permeability	ε_s	Static permittivity
b	Composition constant	M_s	Saturation magnetization	H	External magnetic field
ε_∞	Permittivity at the infinite frequency	f_m	Matching frequency	t_m	Matching thickness

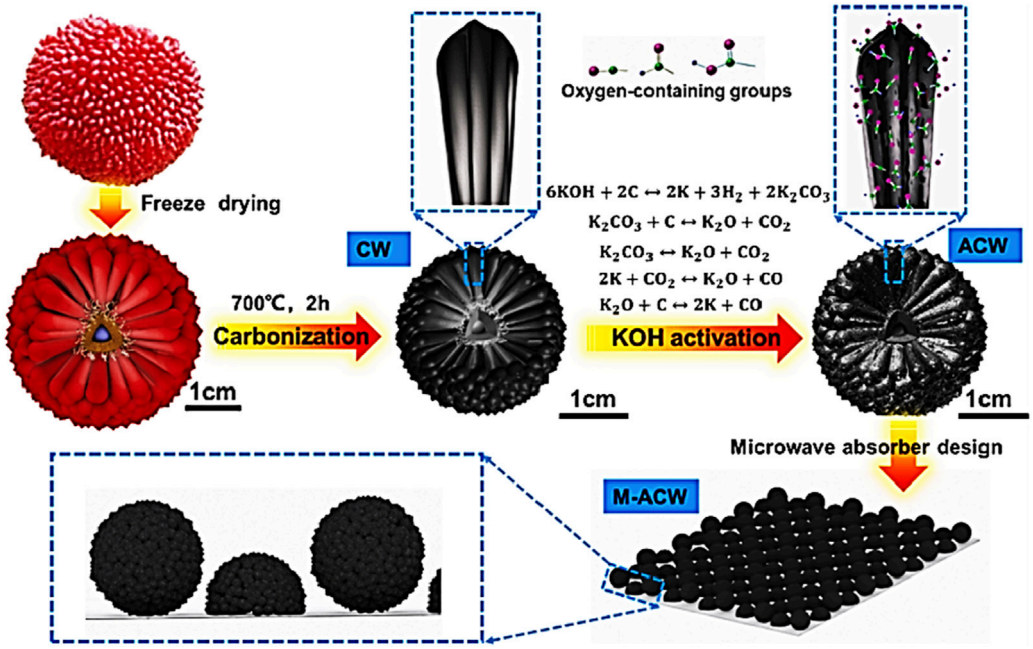

FIGURE 16
Fabrication process of low-frequency ultrabroad bandwidth waxberry metamaterial (Sun et al., 2021).

2014; Yan et al., 2014; Zhou et al., 2015). The nearly perfect absorption, ease of fabrication, lower cost, and small thickness are some advantages of MMAs over conventional absorbers (Sood and Tripathi, 2015; Lee et al., 2016). Despite the many advantages of MMAs, this type of microwave absorber has a narrow absorption bandwidth, which is mainly related to the strong magnetic and electric resonances (Sood and Tripathi, 2015; Cheng et al., 2017a; Xin et al., 2017). To solve this issue, researchers have designed dual, multi, and broadband MMAs with high absorbing performance (Hu et al., 2016; Lian et al., 2016; Rufangura and Sabah, 2016; Wang, 2016). Some researchers have proposed enhancing the bandwidth by employing multi-resonance units with diverse geometric dimensions (Li et al., 2011; Ghosh et al., 2013; Park et al., 2013; Viet et al., 2014). Other researchers have extended the efficient bandwidth by constructing multi-layer absorbers by vertically stacking multiple various metallic resonance structures (Xiong et al., 2013; Yang et al., 2013; Bhattacharyya et al., 2015). Some bandwidth enhancement approaches, including the frequency tunable method and lumped elements loading technique, have also been utilized for bandwidth enhancement (Kim et al., 2016; Zhang et al., 2016). These methods have disadvantages such as increasing unit dimension, greater thickness, and formation difficulty that limit their application. Consequently, there is an urgent need to design a single-layer MMA with high efficiency and broadband absorption (Xin et al., 2017).

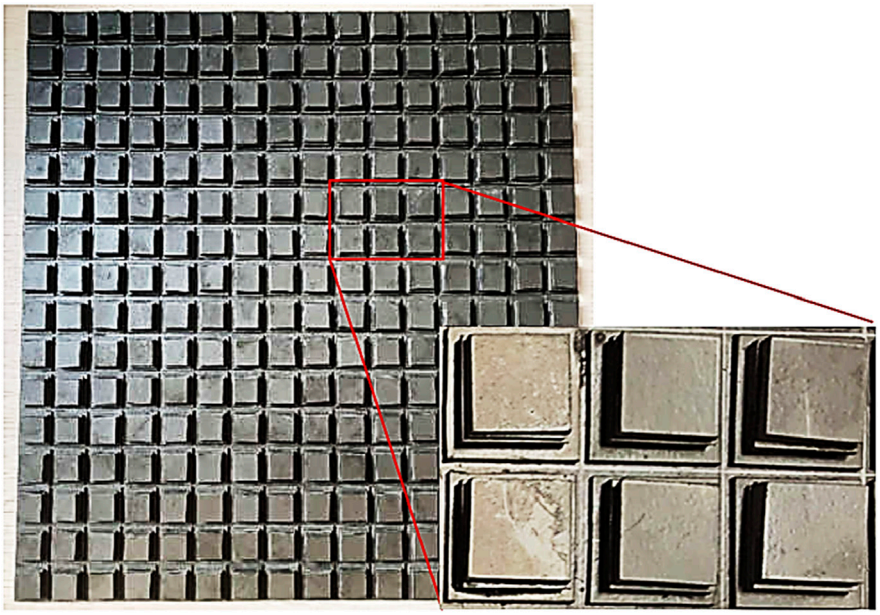

FIGURE 17
Photograph of the fabricated prototype (Ning et al., 2020b).

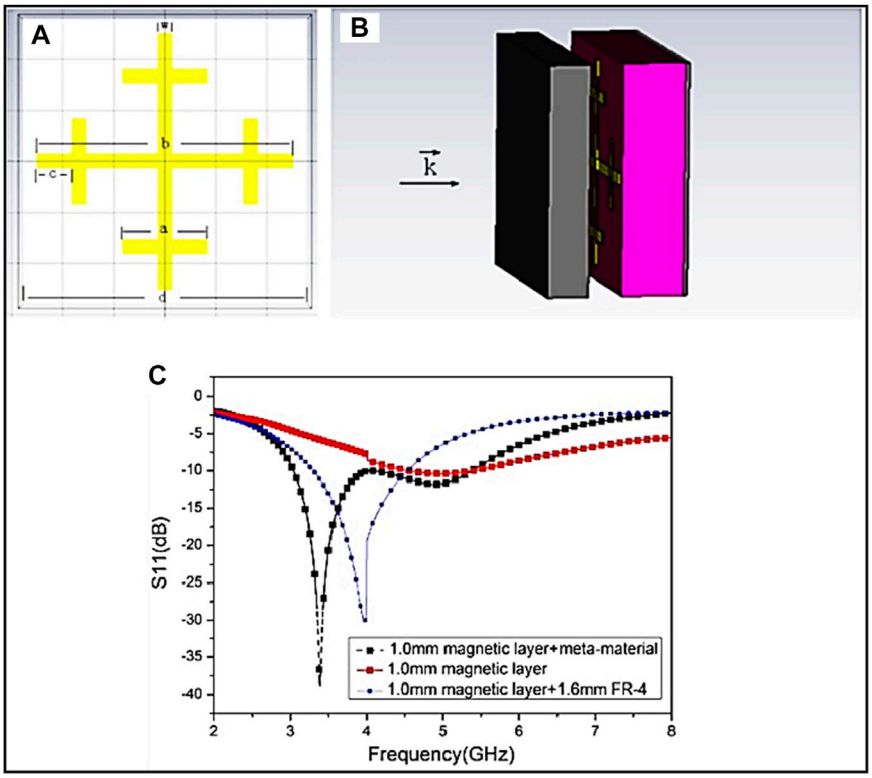

FIGURE 18
(A) Schematic of a metamaterial structure. **(B)** General configuration. **(C)** S11 curves of various structures (Huang et al., 2014).

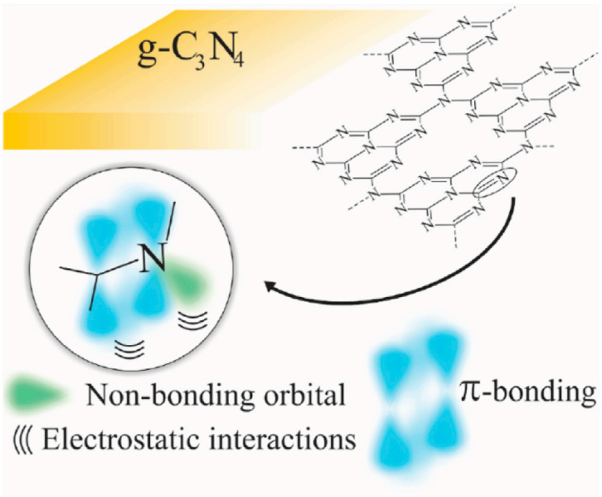

FIGURE 19
Overview of the chemical structure and electrostatic interactions in g-C_3N_4 (Peymanfar et al., 2022).

Sun et al. (2021) fabricated a low-frequency ultra-broad bandwidth metamaterial for microwave absorption based on activated waxberry. Applying natural hierarchical biomass is one solution for the contradiction between electromagnetic loss and impedance matching in microwave absorbers. The metamaterial demonstrated ultrabroad bandwidth properties, with an efficient absorbing band covering 1–40 GHz. An incident-angle independent feature (from 5° to 40°) was also detected. The high performance of this metamaterial was the result of good interface impedance matching of the fabricated metastructure and chemical activation, leading to a high dielectric loss. Additionally, the carbonized waxberry gradient radial microstructure is one essential reason for the broadband microwave absorption (Figure 16).

Xu et al. (2021) also fabricated a metamaterial microwave absorber based on planar indium tin oxide (ITO) and low-loss glass substrates that showed polarization insensitivity, wide operation angle, broad bandwidth, and high absorbing properties. After preparation and conducting relevant assessments such as transmission line theory and equivalent circuit model, the metamaterial showed >90% absorption at 8–20 GHz with a vast angular range from 0 to 60°. In addition, by applying transparent substrates such as quartz glass and soda-lime glass, high optical transmittance (approximately 80%) was achieved. The lower dielectric loss of quartz glass compared to other dielectric substrates indicated that the high microwave absorption mainly contributed to the planar indium tin oxide metamaterial structure.

Ning et al. (2020b) manufactured a step-structured metamaterial electromagnetic absorber composed of magnetic materials including carbonyl iron powder blended in resin. The metamaterial showed >90% electromagnetic absorption in the frequency range of 1.23–19 GHz with a measured thickness of 6 mm. The broadband and strong electromagnetic absorption were mainly related to the structure-induced multi-resonances, the edge diffraction effects of the stepped structures, and the high magnetic loss of the magnetic materials. Additionally, the absorber showed a good angular performance, with incident angles of up to 70° for transverse magnetic (TM)-polarized incidence and 45° for transverse electric (TE) case (Figure 17).

Cheng et al. (2017a) described an ultra-thin broadband microwave absorber based on a magnetic rubber plate and cross-shaped metamaterial structure. Low-frequency absorption was easily achieved by adjusting the geometric specifications of the cross-shaped metamaterial structure and the magnetic rubber plate thickness. The authors reported a broader bandwidth (2.5 GHz) with a thickness of 2 mm. The bandwidth expansion resulted from the overlap of two resonance absorption peaks from the magnetic rubber plate and cross-shaped structure metamaterial, respectively.

Huang et al. (2014) continued their work by proposing a second-order cross-fractal of magnetic materials (Figure 18) to decrease the magnetic material thickness and broaden the bandwidth. The results showed that the prepared MTM thickness decreased to 1 mm, with a bandwidth that broadened by 1.09 GHz compared to the unloaded magnetic

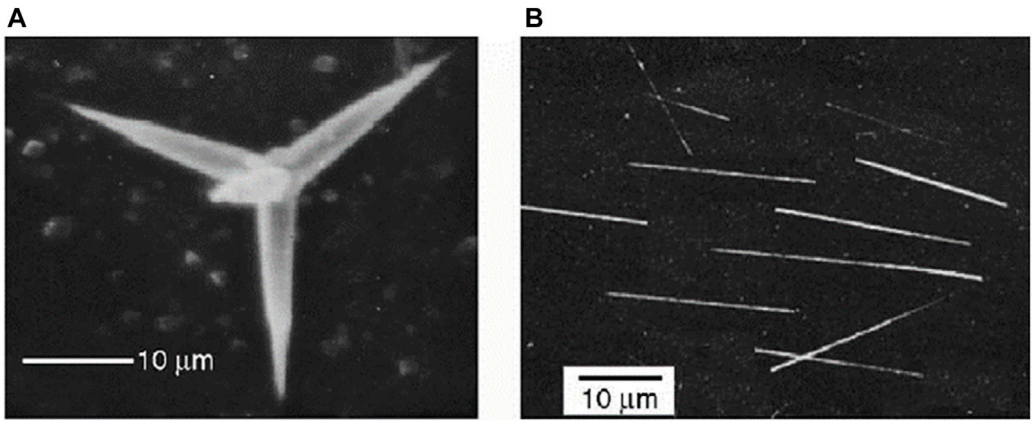

FIGURE 20
(A) SEM images of T-ZnO and **(B)** 1D ZnO whiskers (Zhou et al., 2006).

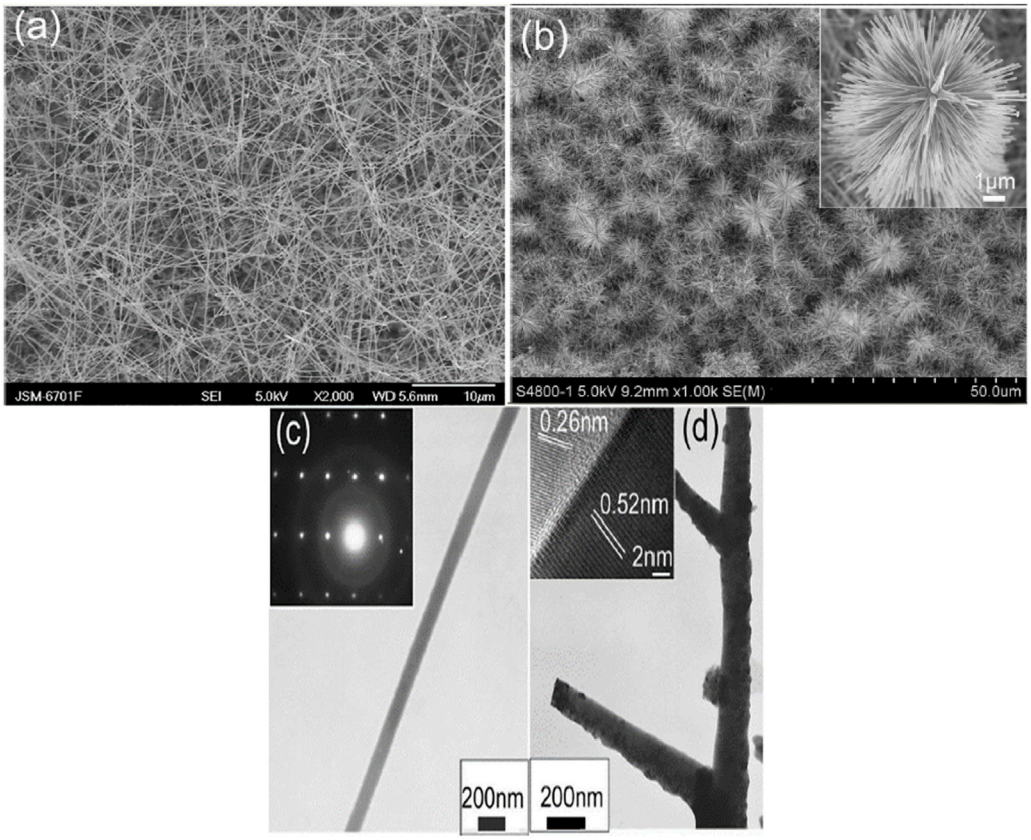

FIGURE 21
SEM images of ZnO **(A)** nanowires and **(B)** nanotrees as well as TEM images of ZnO **(C)** nanowires and **(D)** branches of the nanotrees (Zhuo et al., 2008).

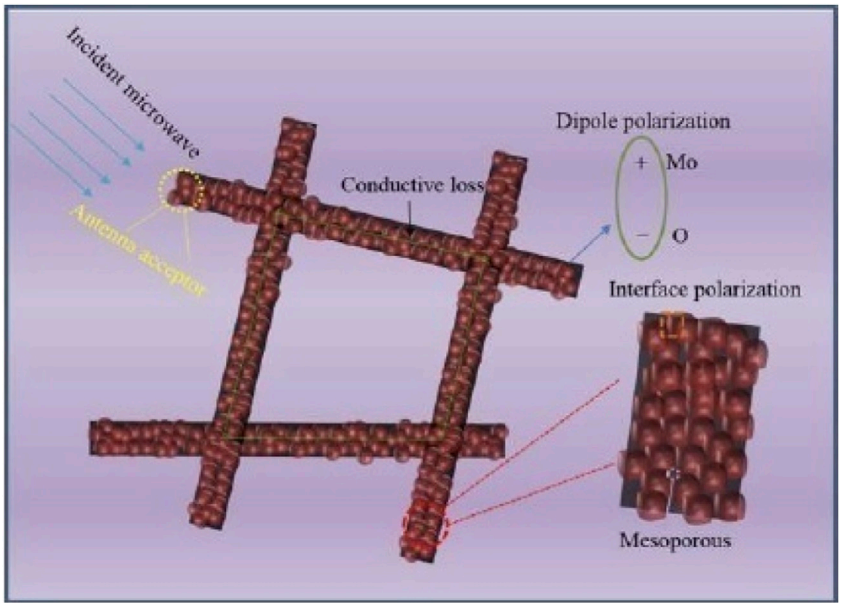

FIGURE 22
Schematic illustration of the microwave-dissipated process in MoO_2/C nanowires (Cheng et al., 2017b).

layer. After analyzing the metamaterial functions, the authors concluded that the MTM possessed two functions, namely, the addition of an extra absorption band and a slightly moved absorption band, due to the magnetic material.

Zhang et al. (2020c) reported the successful fabrication of a metamaterial microwave absorber with high efficiency in the low-frequency regions, especially in the S-band (2–4 GHz). The absorber was formed by stacking layers of metamaterials and magnetic coatings. The results demonstrated that the manufactured metamaterial showed good impedance matching and broadband absorption (2.2–9.5 GHz) by using magnetic materials with high dielectric substrates and well-designed structures.

3.2 Quasi-antennas

A polarized structure under an input electromagnetic wave can induce a secondary field by producing a quasi-antenna structure, producing permeability and improving impedance matching, eventually boosting microwave attenuation.

Electrostatic interactions produced by lone pairs of electrons (non-bonding) on doped heteroatoms, heteroatoms in the polymer backbone, or anti-bonding orbitals containing σ^* and π^*, develop electron hopping, conductive loss, micro currents, polarization paths, secondary fields, and conductive networks. Figure 19 shows the electrostatic susceptibility in g-C_3N_4 (Peymanfar et al., 2022).

The charge flow under an alternating field generates quasi-antennas, creating secondary magnetic fields that interact with and degrade the magnetic part of incident electromagnetic waves, producing permeability, strengthening impedance matching, and promoting microwave absorption (Peymanfar et al., 2022).

The heteroatoms in conjugated structures act as polarization centers and tune the energy gap, regulating conductivity and polarizability. Interestingly, both features can augment the quasi-antenna property in an alternating field. However, the tailored morphology of the dielectric structure plays a crucial role in producing quasi-antennas in an absorbing medium (Peymanfar and Mirkhan, 2022). Under an alternating field, the electron cloud migrates toward the atom with greater electronegativity. Thus, the heteroatom as a polarization center develops quasi-antenna paths, generating secondary magnetic fields, which can be deduced by Oersted's law.

Zhou et al. (2006) studied the microwave-heat transformation of the ZnO whisker and its composite to explain how tetra needle-shaped semiconductor networks absorb microwaves and how quasi-antenna composites create diffuse reflections.

When the material is subjected to an electromagnetic field, the charge concentration at the tips of the T-ZnO whisker needles increases and they function as multipoles, tuned by the incident microwaves, contributing to microwave absorption. Comparison of T-ZnO to 1D ZnO (Figure 20) shows that the former has extremely sharp tips, which contribute to the charge concentration and quasi-antenna effects. Furthermore, the quasi-antenna semiconducting crystalline structures of T-ZnO whiskers emit microwaves with random distributions, resulting in diffuse reflections of incident microwaves.

Cheng et al investigated the microwave-absorbing properties of three-dimensional ZnO micro/nanorod networks. The random distribution of semi-conducting zinc oxide crystals in an isotropic quasi-antenna leads not only to the scattering of incident microwaves and attenuation of EM energy but also acts as microwave receivers by producing vibrating microcurrents in local networks (Li et al., 2010). The vibrating microcurrent induces the vortex magnetic field around the nanotrees, while the alternating magnetic field induces the vortex electric field around itself. The alternating vortex electric and magnetic fields induce each other and then generate EM radiation. This is justified by antenna theory. With the random orientation of these isotropic quasi-antennas, a large part of the EM radiation counteracts each other (Zhuo et al., 2008). Figure 21 shows the SEM and TEM images of the as-synthesized products, in which the nanotrees show isotropic crystal symmetry like isotropic antennas, which may play an important role in microwave attenuation (Zhuo et al., 2008).

By receiving EM energy as an antenna and transforming it into dissipated current, netlike ZnO nanostructures act as a transmitting antenna and transform vibrating current into EM radiation (Li et al., 2010). The microwave-absorbing properties of nanostructured ZnO whiskers were explained by Xiao-Ling et al. (2007) using a quasi-antenna model. Due to their high length-to-diameter (LD) ratio and the n-type semiconductor property, polarized charges are readily formed at the sharp needlepoints of nanostructured ZnO whiskers during EMW transmission. Therefore, at high frequencies, a single leg of ZnO whiskers can be treated as a vibrating electric dipole, and a large number of nanostructured ZnO whiskers can be polarized as a large number of individual radiation sources. According to common knowledge, the established electric dipole is the fundamental cell of antenna radiation.

Cheng et al. designed novel 1D mesoporous MoO_2/C hetero-nanowires. Figure 22 shows the mechanisms to elucidate the superior dielectric loss of the absorber. The 1D nanowires can be considered quasi-antenna acceptors based on the theory of short dipole antennas. Additionally, charge transitions and hopping will form conduction currents along with conjugated nanowires and established networks. This causes Joule-level heating in an alternating EM field. Lastly, interfacial polarization derived from multiple interfaces induced by MoO_2, C, dipole polarization from MoO_2, defects, and remaining heteroatoms convert microwave energy into thermal energy, leading to increased microwave absorption (Cheng et al., 2017b; Hou et al., 2019).

The evaluated mechanisms demonstrate that the metamaterial and quasi-antenna characteristics are efficient mechanisms to be considered in developing conjugated organic polymers to promote their microwave-absorbing features. These features can be inserted into their structures, particularly by modifying their morphology and elemental doping.

4 Conclusion and prospects

An increasing number of studies on EMA in the field of conjugated polymers have demonstrated that these conductive materials are excellent microwave absorbers with wide practical applications due to their remarkable dielectric properties and

lightweight structures. This review examined various methods used to prepare organic polymer structures and explained the effects of morphology and doping on the microwave-absorbing ability of conductive polymers. Furthermore, the mechanisms resulting in the microwave-absorbing characteristics of pure carbon-based absorbers and other conjugated organic polymers containing heteroatoms were dissected and the doped and composite structures were evaluated. Due to their superior electrical contact and rapid electron conduction, this class of materials has attracted considerable interest for microwave absorption and shielding structures as well as energy conversion and storage. Since the conductive and polarization losses are the predominant characteristics associated with the microwave absorption of conjugated organic polymers, the discussion of morphology (wires, nanotubes, fiber, 2D, fabric, etc.) and orbital orientations facilitating the charge transitions are determinative in microwave-absorbing performance. Strong dielectric characteristics diminish impedance matching, reducing the propagation of incident waves into the absorbing medium, efficient bandwidth, and microwave attenuation. Therefore, these types of materials are equipped with magnetic components to establish permeability and increase microwave absorption and impedance matching, complicating the experimental process. Doping (elemental, oxidative, or reductive) is another way to tune the energy band gap and charge accumulation in HOMO, regulating polarization and conductive losses. Metamaterial and quasi-antenna mechanisms are observed in dielectric structures with unique morphologies. The charge circuits in conjugated structures and conductive networks can generate secondary fields; the polarized structures with special morphologies can form quasi-antenna structures, creating permeability and improving impedance matching. More importantly, the doped atoms can act as polarization centers in which higher electronegativity attracts electron clouds and enhances charge accumulation, promoting dipole polarization and quasi-antenna features. However, some conjugated organic polymers have complex synthetic routes, which limits practical applications. To address this obstacle, pyrolyzed biomass-derived materials have been widely applied as attainable and affordable precursors to fabricate microwave-absorbing materials. This review sheds new light on architecting conjugated organic polymers with unique morphology and considers the mechanisms of metamaterials and quasi-antennas to enhance the microwave-absorbing capability to provide practical microwave refiners. More importantly, the reported results clarified that doping is a facile solution to promote the microwave-absorbing characteristics of conjugated structures.

Author contributions

RP: project administration, supervision, methodology, visualization, resources, conceptualization, data curation, and writing—review and editing; HD: writing—review and editing; ES-Z: writing—review and drawing schematic diagram (Figure 1); MH: writing—review; SD: writing—review; NA-R: writing—review; HG: project administration, supervision, and writing—review and editing; AM: project administration and resources; GJ: review and writing—editing; BA: writing—review and editing.

Conflict of interest

Authors RP and AM were employed by Peykareh Enterprise Development Co.

The remaining authors declare that the research was conducted in the absence of any commercial or financial relationships that could be construed as a potential conflict of interest.

Publisher's note

References

Alici, K. B., and Özbay, E. (2007). Radiation properties of a split ring resonator and monopole composite. *Phys. status solidi (b)* 244, 1192–1196. doi:10.1002/pssb.200674505

Amireddy, K. K., Balasubramaniam, K., and Rajagopal, P. (2016). Holey-structured metamaterial lens for subwavelength resolution in ultrasonic characterization of metallic components. *Appl. Phys. Lett.* 108, 224101. doi:10.1063/1.4950967

Atassi, Y., and Fun, X. (2020). Mesoporous carbon decorated with FeCoNi/polyaniline/polypyrrole towards lightweight and efficient microwave absorption coating. *J. Mater. Sci. Mater. Electron.* 31, 21948–21958. doi:10.1007/s10854-020-04698-5

Aydin, K., Bulu, I., and Ozbay, E. (2007). Subwavelength resolution with a negative-index metamaterial superlens. *Appl. Phys. Lett.* 90, 254102. doi:10.1063/1.2750393

Bhattacharyya, S., Ghosh, S., Chaurasiya, D., and Srivastava, K. V. (2015). Bandwidth-enhanced dual-band dual-layer polarization-independent ultra-thin metamaterial absorber. *Appl. Phys. A* 118, 207–215. doi:10.1007/s00339-014-8908-z

Bi, Y., Ma, M., Liao, Z., Tong, Z., Chen, Y., Wang, R., et al. (2022). One-dimensional Ni@Co/C@PPy composites for superior electromagnetic wave absorption. *J. Colloid Interface Sci.* 605, 483–492. doi:10.1016/j.jcis.2021.07.050

Bian, B., Liu, S., Wang, S., Kong, X., Guo, Y., Zhao, X., et al. (2013). Cylindrical optimized nonmagnetic concentrator with minimized scattering. *Opt. Express* 21, A231–A240. doi:10.1364/oe.21.00a231

Cao, M.-S., Song, W.-L., Hou, Z.-L., Wen, B., and Yuan, J. (2010). The effects of temperature and frequency on the dielectric properties, electromagnetic interference shielding and microwave-absorption of short carbon fiber/silica composites. *Carbon* 48, 788–796. doi:10.1016/j.carbon.2009.10.028

Cao, M.-S., Wang, X.-X., Cao, W.-Q., and Yuan, J. (2015). Ultrathin graphene: Electrical properties and highly efficient electromagnetic interference shielding. *J. Mater. Chem. C* 3, 6589–6599. doi:10.1039/c5tc01354b

Chen, H.-T., Padilla, W. J., Zide, J. M., Gossard, A. C., Taylor, A. J., and Averitt, R. D. (2006). Active terahertz metamaterial devices. *Nature* 444, 597–600. doi:10.1038/nature05343

Chen, J., Zheng, J., Huang, Q., Wang, F., and Ji, G. (2021). Enhanced microwave absorbing ability of carbon fibers with embedded FeCo/$CoFe_2O_4$ nanoparticles. *ACS Appl. Mater. Interfaces* 13, 36182–36189. doi:10.1021/acsami.1c09430

Chen, J., Zheng, J., Wang, F., Huang, Q., and Ji, G. (2021). Carbon fibers embedded with FeIII-MOF-5-derived composites for enhanced microwave absorption. *Carbon* 174, 509–517. doi:10.1016/j.carbon.2020.12.077

Chen, X., Liu, H., Hu, D., Liu, H., and Ma, W. (2021). Recent advances in carbon nanotubes-based microwave absorbing composites. *Ceram. Int.* 47, 23749–23761. doi:10.1016/j.ceramint.2021.05.219

Cheng, J., Zhang, H., Ning, M., Raza, H., Zhang, D., Zheng, G., et al. (2022). *Advanced functional materials*, 2200123.

Cheng, Y., He, B., Zhao, J., and Gong, R. (2017). Ultra-thin low-frequency broadband microwave absorber based on magnetic medium and metamaterial. *J. Electron. Mater.* 46, 1293–1299. doi:10.1007/s11664-016-5115-z

Cheng, Y., Meng, W., Li, Z., Zhao, H., Cao, J., Du, Y., et al. (2017). Towards outstanding dielectric consumption derived from designing one-dimensional mesoporous MoO_2/C hybrid heteronanowires. *J. Mater. Chem. C* 5, 8981–8987. doi:10.1039/c7tc02835k

Colombi, A., Roux, P., Guenneau, S., and Rupin, M. (2015). Directional cloaking of flexural waves in a plate with a locally resonant metamaterial. *J. Acoust. Soc. Am.* 137, 1783–1789. doi:10.1121/1.4915004

Cummer, S. A., Popa, B.-I., Schurig, D., Smith, D. R., and Pendry, J. (2006). Full-wave simulations of electromagnetic cloaking structures. *Phys. Rev. E* 74, 036621. doi:10.1103/physreve.74.036621

Das, T. K., and Prusty, S. (2012). Review on conducting polymers and their applications. *Polymer-plastics Technol. Eng.* 51, 1487–1500. doi:10.1080/03602559.2012.710697

Diao, J., Cai, Z., Xia, L., Wang, Z., Yin, Z., Liu, X., et al. (2021). High-performance microwave absorption of 3D Bi2Te2.7Se0.3/Graphene foam. *Carbon* 183, 702–710. doi:10.1016/j.carbon.2021.07.049

Ding, F., Cui, Y., Ge, X., Jin, Y., and He, S. (2012). Ultra-broadband microwave metamaterial absorber. *Appl. Phys. Lett.* 100, 103506. doi:10.1063/1.3692178

Ding, J., Wang, L., Zhao, Y., Xing, L., Yu, X., Chen, G., et al. (2019). Boosted interfacial polarization from Multishell TiO_2 @Fe_3O_4 @PPy Heterojunction for enhanced microwave absorption. *Small* 15, 1902885. doi:10.1002/smll.201902885

Duan, X., Chen, S., Liu, W., Cheng, H., Li, Z., and Tian, J. (2014). Polarization-insensitive and wide-angle broadband nearly perfect absorber by tunable planar metamaterials in the visible regime. *J. Opt.* 16, 125107. doi:10.1088/2040-8978/16/12/125107

Duan, Y., Xiao, Z., Yan, X., Gao, Z., Tang, Y., Hou, L., et al. (2018). Enhanced electromagnetic microwave absorption property of Peapod-like MnO@carbon nanowires. *ACS Appl. Mater. interfaces* 10, 40078–40087. doi:10.1021/acsami.8b11395

Englert, C., Brendel, J. C., Majdanski, T. C., Yildirim, T., Schubert, S., Gottschaldt, M., et al. (2018). Pharmapolymers in the 21st century: Synthetic polymers in drug delivery applications. *Prog. Polym. Sci.* 87, 107–164. doi:10.1016/j.progpolymsci.2018.07.005

Enoch, S., Tayeb, G., Sabouroux, P., Guérin, N., and Vincent, P. (2002). A metamaterial for directive Emission. *Phys. Rev. Lett.* 89, 213902. doi:10.1103/physrevlett.89.213902

Ghosh, S., Bhattacharyya, S., and Srivastava, K. V. (2013). *Prog. Electromag. Res. Symposium Proc.*, 1097–1101.

Gu, H., Xu, X., Dong, M., Xie, P., Shao, Q., Fan, R., et al. (2019). Carbon nanospheres induced high negative permittivity in nanosilver-polydopamine metacomposites. *Carbon* 147, 550–558. doi:10.1016/j.carbon.2019.03.028

Guan, H., Wang, Q., Wu, X., Pang, J., Jiang, Z., Chen, G., et al. (2021). Biomass derived porous carbon (BPC) and their composites as lightweight and efficient microwave absorption materials. *Compos. Part B Eng.* 207, 108562. doi:10.1016/j.compositesb.2020.108562

Gunwant, D., and Vedrtnam, A. (2021). Microwave absorbing properties of carbon fiber based materials: A review and prospective. *J. Alloys Compd.* 881, 160572. doi:10.1016/j.jallcom.2021.160572

Hao, J., Wang, J., Liu, X., Padilla, W. J., Zhou, L., and Qiu, M. (2010). High performance optical absorber based on a plasmonic metamaterial. *Appl. Phys. Lett.* 96, 251104. doi:10.1063/1.3442904

Hou, T., Jia, Z., Feng, A., Zhou, Z., Liu, X., Lv, H., et al. (2021). Hierarchical composite of biomass derived magnetic carbon framework and phytic acid doped polyanilne with prominent electromagnetic wave absorption capacity. *J. Mater. Sci. Technol.* 68, 61–69. doi:10.1016/j.jmst.2020.06.046

Hou, T., Wang, B., Jia, Z., Wu, H., Lan, D., Huang, Z., et al. (2019). A review of metal oxide-related microwave absorbing materials from the dimension and morphology perspective. *J. Mater. Sci. Mater. Electron.* 30, 10961–10984. doi:10.1007/s10854-019-01537-0

Hu, D., Wang, H., Tang, Z., Zhang, X., and Zhu, Q. (2016). *Appl. Phys. A* 122, 1–7.

Huang, D., Kang, F., Dong, C., Zhou, Z., Liu, X., and Ding, H. (2014). A second-order cross fractal meta-material structure used in low-frequency microwave absorbing materials. *Appl. Phys. A* 115, 627–635. doi:10.1007/s00339-014-8374-7

Huynen, I. (2022). *Front. Mater.* 9, 1040753.

Ibrahim, I. R., Matori, K. A., Ismail, I., Awang, Z., Rusly, S. N. A., Nazlan, R., et al. (2020). *Sci. Rep.* 10, 1–14.

Jia, Z., Lan, D., Lin, K., Qin, M., Kou, K., Wu, G., et al. (2018). Progress in low-frequency microwave absorbing materials. *J. Mater. Sci. Mater. Electron.* 29, 17122–17136. doi:10.1007/s10854-018-9909-z

Jiao, Y., Wu, F., Xie, A., Wu, L., Zhao, W., Zhu, X., et al. (2020). Electrically conductive conjugate microporous polymers (CMPs) via confined polymerization of pyrrole for electromagnetic wave absorption. *Chem. Eng. J.* 398, 125591. doi:10.1016/j.cej.2020.125591

Kim, H. K., Lee, D., and Lim, S. (2016). Frequency-tunable metamaterial absorber using a varactor-loaded fishnet-like resonator. *Appl. Opt.* 55, 4113–4118. doi:10.1364/ao.55.004113

Kumar, R., Sahoo, S., Joanni, E., Singh, R. K., Tan, W. K., Kar, K. K., et al. (2021). Recent progress on carbon-based composite materials for microwave electromagnetic interference shielding. *Carbon* 177, 304–331. doi:10.1016/j.carbon.2021.02.091

Kurihara, H., Hirai, Y., Takizawa, K., Iwata, T., and Hashimoto, O. (2005). An improvement of Communication environment for ETC system by using transparent EM wave absorber. *IEICE Trans. Electron.* 88, 2350–2357. doi:10.1093/ietele/e88-c.12.2350

Lalan, V., and Ganesanpotti, S. (2020). Broadband electromagnetic response and enhanced microwave absorption in carbon black and magnetic Fe3O4 nanoparticles reinforced Polyvinylidenefluoride composites. *J. Electron. Mater.* 49, 1666–1676. doi:10.1007/s11664-019-07635-3

Landy, N. I., Sajuyigbe, S., Mock, J. J., Smith, D. R., and Padilla, W. J. (2008). Perfect metamaterial absorber. *Phys. Rev. Lett.* 100, 207402. doi:10.1103/physrevlett.100.207402

Lee, D., Sung, H.-K., and Lim, S. (2016). *Appl. Phys. B* 122, 1–8.

Lei, Y., Ding, M., Wu, H., Yin, D., Li, Y., Jiang, B., et al. (2022). *Ppy composites with a core-shell structure*.

Li, H., Huang, Y., Sun, G., Yan, X., Yang, Y., Wang, J., et al. (2010). Directed Growth and microwave absorption property of crossed ZnO netlike micro-/nanostructures. *J. Phys. Chem. C* 114, 10088–10091. doi:10.1021/jp100341h

Li, J.-S., Huang, H., Zhou, Y.-J., Zhang, C.-Y., and Li, Z.-T. (2017). Research progress of graphene-based microwave absorbing materials in the last decade. *J. Mater. Res.* 32, 1213–1230. doi:10.1557/jmr.2017.80

Li, L., Yang, Y., and Liang, C. (2011). A wide-angle polarization-insensitive ultra-thin metamaterial absorber with three resonant modes. *J. Appl. Phys.* 110, 063702. doi:10.1063/1.3638118

Li, X., Qiao, L., Shi, H., Chai, G., Wang, T., and Wang, J. (2022). *Front. Mater.* 9, 1054725.

Li, X., Wang, L., You, W., Xing, L., Yu, X., Li, Y., et al. (2019). Morphology-controlled synthesis and excellent microwave absorption performance of $ZnCo_2O_4$ nanostructures *via* a self-assembly process of flake units. *Nanoscale* 11, 2694–2702. doi:10.1039/c8nr08601j

Lian, Y., Ren, G., Liu, H., Gao, Y., Zhu, B., Wu, B., et al. (2016). Dual-band near-infrared plasmonic perfect absorber assisted by strong coupling between bright-dark nanoresonators. *Opt. Commun.* 380, 267–272. doi:10.1016/j.optcom.2016.06.024

Liu, D., Du, Y., Xu, P., Wang, F., Wang, Y., Cui, L., et al. (2021). Rationally designed hierarchical N-doped carbon nanotubes wrapping waxberry-like Ni@C microspheres for efficient microwave absorption. *J. Mater. Chem. A* 9, 5086–5096. doi:10.1039/d0ta10942h

Lou, Z., Wang, Q., Kara, U. I., Mamtani, R. S., Zhou, X., Bian, H., et al. (2022). *Nano-micro Lett.* 14, 1–16.

Luo, J., and Gao, D. (2014). Synthesis and microwave absorption properties of PPy/Co nanocomposites. *J. magnetism magnetic Mater.* 368, 82–86. doi:10.1016/j.jmmm.2014.05.009

Lv, H., Yang, Z., Liu, B., Wu, G., Lou, Z., Fei, B., et al. (2021). A flexible electromagnetic wave-electricity harvester. *Nat. Commun.* 12, 834. doi:10.1038/s41467-021-21103-9

Lv, H., Yang, Z., Pan, H., and Wu, R. (2022). Electromagnetic absorption materials: Current progress and new frontiers. *Prog. Mater. Sci.* 127, 100946. doi:10.1016/j.pmatsci.2022.100946

Lv, H., Yang, Z., Xu, H., Wang, L., and Wu, R. (2020). An electrical Switch-Driven flexible electromagnetic absorber. *Adv. Funct. Mater.* 30, 1907251. doi:10.1002/adfm.201907251

Mahmoodi, M., Aslibeiki, B., Peymanfar, D., and Naghshara, H. (2022). *Front. Mater.*, 750.

Maitz, M. F. (2015). Applications of synthetic polymers in clinical medicine. *Biosurface Biotribology* 1, 161–176. doi:10.1016/j.bsbt.2015.08.002

Meng, F., Wang, H., Huang, F., Guo, Y., Wang, Z., Hui, D., et al. (2018). Graphene-based microwave absorbing composites: A review and prospective. *Compos. Part B Eng.* 137, 260–277. doi:10.1016/j.compositesb.2017.11.023

Mo, Z., Yang, R., Lu, D., Yang, L., Hu, Q., Li, H., et al. (2019). Lightweight, three-dimensional carbon Nanotube@TiO2 sponge with enhanced microwave absorption performance. *Carbon* 144, 433–439. doi:10.1016/j.carbon.2018.12.064

Munir, A. (2017). Microwave radar absorbing properties of Multiwalled carbon nanotubes polymer composites: A review. *Adv. Polym. Technol.* 36, 362–370. doi:10.1002/adv.21617

Ning, J., Dong, S., Luo, X., Chen, K., Zhao, J., Jiang, T., et al. (2020). Ultra-broadband microwave absorption by ultra-thin metamaterial with stepped structure induced multi-resonances. *Results Phys.* 18, 103320. doi:10.1016/j.rinp.2020.103320

Ning, M., Man, Q., Tan, G., Lei, Z., Li, J., and Li, R.-W. (2020). Ultrathin MoS_2 nanosheets encapsulated in Hollow carbon spheres: A case of a dielectric absorber with optimized impedance for efficient microwave absorption. *ACS Appl. Mater. interfaces* 12, 20785–20796. doi:10.1021/acsami.9b20433

Olmedo, L., Hourquebie, P., and Jousse, F. (1993). Microwave absorbing materials based on conducting polymers. *Adv. Mater.* 5, 373–377. doi:10.1002/adma.19930050509

Olmedo, L., Hourquebie, P., and Jousse, F. (1995). Microwave properties of conductive polymers. *Synth. Met.* 69, 205–208. doi:10.1016/0379-6779(94)02417-w

Park, J. W., Van Tuong, P., Rhee, J. Y., Kim, K. W., Jang, W. H., Choi, E. H., et al. (2013). Multi-band metamaterial absorber based on the arrangement of donut-type resonators. *Opt. express* 21, 9691–9702. doi:10.1364/oe.21.009691

Pattanayak, S. S., Laskar, S., and Sahoo, S. (2021). Progress on agricultural residue-based microwave absorber: A review and prospects. *J. Mater. Sci.* 56, 4097–4119. doi:10.1007/s10853-020-05557-8

Peymanfar, R., Afghahi, S. S. S., and Javanshir, S. (2019). Preparation and investigation of structural, magnetic, and microwave absorption properties of a $SrAl_{1.3}Fe_{10.7}O_{19}$/Multiwalled carbon nanotube nanocomposite in X and ku-band frequencies. *J. Nanosci. Nanotechnol.* 19, 3911–3918. doi:10.1166/jnn.2019.16311

Peymanfar, R., Ahmadi, A., and Selseleh-Zakerin, E. (2020). Evaluation of the size and medium effects on the microwave absorbing, magnetic, electromagnetic shielding, and optical properties using CuCo2S4 nanoparticles. *J. Alloys Compd.* 848, 156453. doi:10.1016/j.jallcom.2020.156453

Peymanfar, R., Ahmadi, A., Selseleh-Zakerin, E., Ghaffari, A., Mojtahedi, M. M., and Sharifi, A. (2021). Electromagnetic and optical characteristics of wrinkled Ni nanostructure coated on carbon microspheres. *Chem. Eng. J.* 405, 126985. doi:10.1016/j.cej.2020.126985

Peymanfar, R., Ahmadi, M., and Javanshir, S. (2019). Tailoring GO/$BaFe_{12}O_{19}$/$La_{0.5}Sr_{0.5}MnO_3$ ternary nanocomposite and investigation of its microwave characteristics. *Mater. Res. Express* 6, 085063. doi:10.1088/2053-1591/ab1fb3

Peymanfar, R., Ershad, Z. S., Selseleh-Zakerin, E., and Tavassoli, S. H. (2022). *Ceram. Int*.

Peymanfar, R., and Fazlalizadeh, F. (2021). Fabrication of expanded carbon microspheres/ZnAl2O4 nanocomposite and investigation of its microwave, magnetic, and optical performance. *J. Alloys Compd.* 854, 157273. doi:10.1016/j.jallcom.2020.157273

Peymanfar, R., and Fazlalizadeh, F. (2020). Microwave absorption performance of ZnAl2O4. *Chem. Eng. J.* 402, 126089. doi:10.1016/j.cej.2020.126089

Peymanfar, R., and Ghorbanian-Gezaforodi, S. (2021). Functionalized carbonized monarch butterfly wing scales (FCBW) ornamented by β-$Co(OH)_2$ nanoparticles: An investigation on its microwave, magnetic, and optical characteristics. *Nanotechnology* 32, 195201. doi:10.1088/1361-6528/abe0e4

Peymanfar, R., and Ghorbanian-Gezaforodi, S. (2020). Preparation of graphite-like carbon nitride (g-C_3N_4)/$NiCo_2S_4$ nanocomposite toward salient microwave characteristics and evaluation of medium influence on its microwave features. *Nanotechnology* 31, 495202. doi:10.1088/1361-6528/abb2c0

Peymanfar, R., Javanshir, S., Naimi-Jamal, M. R., and Cheldavi, A. (2019). *Mater. Res. Express* 6, 0850e0859.

Peymanfar, R., Javanshir, S., Naimi-Jamal, M. R., Cheldavi, A., and Esmkhani, M. (2019). Preparation and characterization of MWCNT/Zn0.25Co0.75Fe2O4 nanocomposite and investigation of its microwave absorption properties at X-band frequency using Silicone rubber polymeric matrix. *J. Electron. Mater.* 48, 3086–3095. doi:10.1007/s11664-019-07065-1

Peymanfar, R., Javanshir, S., Naimi-Jamal, M. R., and Tavassoli, S. H. (2021). Morphology and medium influence on microwave characteristics of nanostructures: A review. *J. Mater. Sci.* 56, 17457–17477. doi:10.1007/s10853-021-06394-z

Peymanfar, R., Keykavous-Amand, S., Abadi, M. M., and Yassi, Y. (2020). A novel approach toward reducing energy consumption and promoting electromagnetic interference shielding efficiency in the buildings using Brick/polyaniline nanocomposite. *Constr. Build. Mater.* 263, 120042. doi:10.1016/j.conbuildmat.2020.120042

Peymanfar, R., and Mirkhan, A. (2022). Biomass-derived materials: Promising, affordable, capable, simple, and lightweight microwave absorbing structures. *Chem. Eng. J.* 446, 136903. doi:10.1016/j.cej.2022.136903

Peymanfar, R., Mohammadi, A., and Javanshir, S. (2020). Preparation of graphite-like carbon nitride/polythiophene nanocomposite and investigation of its optical and microwave absorbing characteristics. *Compos. Commun.* 21, 100421. doi:10.1016/j.coco.2020.100421

Peymanfar, R., and Moradi, F. (2020). Functionalized carbon microfibers (biomass-derived) ornamented by Bi_2S_3 nanoparticles: An investigation on their microwave, magnetic, and optical characteristics. *Nanotechnology* 32, 065201. doi:10.1088/1361-6528/abc2ec

Peymanfar, R., Norouzi, F., and Javanshir, S. (2018). A novel approach to prepare one-pot Fe/PPy nanocomposite and evaluation of its microwave, magnetic, and optical performance. *Mater. Res. Express* 6, 035024. doi:10.1088/2053-1591/aaf709

Peymanfar, R., Selseleh-Zakerin, E., Ahmadi, A., Sharifi, A., and Mojtahedi, M. M. (2021). Regulating microwave absorption and energy bandgap using cauliflower-like polyaniline coated on La0.8Sr0.2FeO3 nanoparticles. *J. Mater. Sci. Mater. Electron.* 32, 25679–25687. doi:10.1007/s10854-020-04203-y

Peymanfar, R., Selseleh-Zakerin, E., and Ahmadi, A. (2021). Tailoring energy band gap and microwave absorbing features of graphite-like carbon nitride (g-C3N4). *J. Alloys Compd.* 867, 159039. doi:10.1016/j.jallcom.2021.159039

Peymanfar, R., Selseleh-Zakerin, E., Ahmadi, A., and Tavassoli, S. H. (2021). *Sci. Rep.* 11, 1–15.

Qiao, M., Lei, X., Ma, Y., Tian, L., Su, K., and Zhang, Q. (2016). Well-defined core–shell Fe_3O_4@Polypyrrole composite microspheres with tunable shell thickness: Synthesis and their superior microwave absorption performance in the ku band. *Industrial Eng. Chem. Res.* 55, 6263–6275. doi:10.1021/acs.iecr.5b04814

Qin, F., and Brosseau, C. (2012). *J. Appl. Phys.* 111, 4.

Rajput, A., and Srivastava, K. V. (2014). Design of a two-dimensional metamaterial cloak with minimum scattering using a quadratic transformation function. *J. Appl. Phys.* 116, 124501. doi:10.1063/1.4893480

Rufangura, P., and Sabah, C. (2016). Wide-band polarization independent perfect metamaterial absorber based on concentric rings topology for solar cells application. *J. Alloys Compd.* 680, 473–479. doi:10.1016/j.jallcom.2016.04.162

Sabah, C., and Uckun, S. (2009). *Prog. Electromagn. Res.* 91, 349–364. doi:10.2528/pier09031306

Schurig, D., Mock, J. J., Justice, B., Cummer, S. A., Pendry, J. B., Starr, A. F., et al. (2006). Metamaterial electromagnetic cloak at microwave frequencies. *Science* 314, 977–980. doi:10.1126/science.1133628

Soares, B. G., Barra, G. M., and Indrusiak, T. (2021). Conducting polymeric composites based on Intrinsically conducting polymers as electromagnetic interference shielding/microwave absorbing materials—a review. *J. Compos. Sci.* 5, 173. doi:10.3390/jcs5070173

Song, Y., Yin, F., Zhang, C., Guo, W., Han, L., and Yuan, Y. (2021). *Nano-micro Lett.* 13, 1–16.

Song, Z., Xie, J., Zhou, P., Wang, X., Liu, T., and Deng, L. (2013). Toughened polymer composites with flake carbonyl iron powders and their electromagnetic/absorption properties. *J. alloys Compd.* 551, 677–681. doi:10.1016/j.jallcom.2012.11.065

Sood, D., and Tripathi, C. (2015). A wideband ultrathin low profile metamaterial microwave absorber. *Microw. Opt. Technol. Lett.* 57, 2723–2728. doi:10.1002/mop.29428

Sun, X., Wang, Z., Wang, S., Ning, Y., Yang, M., Yang, S., et al. (2021). Ultrabroadband and low-frequency microwave absorption based on activated waxberry metamaterial. *Chem. Eng. J.* 422, 130142. doi:10.1016/j.cej.2021.130142

Tak, J., Jin, Y., and Choi, J. (2016). A dual-band metamaterial microwave absorber. *Microw. Opt. Technol. Lett.* 58, 2052–2057. doi:10.1002/mop.29977

Tian, C., Du, Y., Xu, P., Qiang, R., Wang, Y., Ding, D., et al. (2015). Constructing Uniform core–shell PPy@PANI composites with tunable shell thickness toward enhancement in microwave absorption. *ACS Appl. Mater. interfaces* 7, 20090–20099. doi:10.1021/acsami.5b05259

Viet, D., Hien, N., Tuong, P., Minh, N., Trang, P., Le, L., et al. (2014). Perfect absorber metamaterials: Peak, multi-peak and broadband absorption. *Opt. Commun.* 322, 209–213. doi:10.1016/j.optcom.2014.02.037

Wang, B.-X. (2016). *IEEE J. Sel. Top. Quantum Electron.* 23, 1–7.

Wang, F., Liu, Y., Zhao, H., Cui, L., Gai, L., Han, X., et al. (2022). Controllable seeding of nitrogen-doped carbon nanotubes on three-dimensional Co/C foam for enhanced dielectric loss and microwave absorption characteristics. *Chem. Eng. J.* 450, 138160. doi:10.1016/j.cej.2022.138160

Wang, F., Wang, N., Han, X., Liu, D., Wang, Y., Cui, L., et al. (2019). Core-shell FeCo@carbon nanoparticles encapsulated in polydopamine-derived carbon nanocages for efficient microwave absorption. *Carbon* 145, 701–711. doi:10.1016/j.carbon.2019.01.082

Wang, J., Liu, L., Jiao, S., Ma, K., Lv, J., and Yang, J. (2020). Hierarchical carbon Fiber@MXene@MoS_2 core-sheath synergistic microstructure for tunable and efficient microwave absorption. *Adv. Funct. Mater.* 30, 2002595. doi:10.1002/adfm.202002595

Wang, L., Yu, X., Li, X., Zhang, J., Wang, M., and Che, R. (2019). Conductive-network enhanced microwave absorption performance from carbon coated defect-rich Fe2O3 anchored on multi-wall carbon nanotubes. *Carbon* 155, 298–308. doi:10.1016/j.carbon.2019.07.049

Wang, Y., Du, Y., Xu, P., Qiang, R., and Han, X. (2017). Recent advances in conjugated polymer-based microwave absorbing materials. *Polymers* 9, 29. doi:10.3390/polym9010029

Wang, Y. (2014). Microwave absorbing materials based on polyaniline composites: A review. *Int. J. Mater. Res.* 105, 3–12. doi:10.3139/146.110996

Wu, F., Yang, K., Li, Q., Shah, T., Ahmad, M., Zhang, Q., et al. (2021). Biomass-derived 3D magnetic porous carbon fibers with a helical/chiral structure toward superior microwave absorption. *Carbon* 173, 918–931. doi:10.1016/j.carbon.2020.11.088

Wu, Y., Zhao, Y., Zhou, M., Tan, S., Peymanfar, R., Aslibeiki, B., et al. (2022). *Nano-micro Lett.* 14, 1–17.

Xiao-Ling, S., Jie, Y., Wei, Z., Ji-Li, R., and Mao-Sheng, C. (2007). Preparation and dielectric properties of nanostructured ZnO whiskers. *Chin. Phys. Lett.* 24, 2994–2997. doi:10.1088/0256-307x/24/10/078

Xin, W., Binzhen, Z., Wanjun, W., Junlin, W., and Junping, D. (2017). Design and characterization of an Ultrabroadband metamaterial microwave absorber. *IEEE Photonics J.* 9, 1–13. doi:10.1109/jphot.2017.2700056

Xiong, H., Hong, J.-S., Luo, C.-M., and Zhong, L.-L. (2013). An ultrathin and broadband metamaterial absorber using multi-layer structures. *J. Appl. Phys.* 114, 064109. doi:10.1063/1.4818318

Xu, J., Fan, Y., Su, X., Guo, J., Zhu, J., Fu, Q., et al. (2021). Broadband and wide angle microwave absorption with optically transparent metamaterial. *Opt. Mater.* 113, 110852. doi:10.1016/j.optmat.2021.110852

Xu, X., Wang, G., Wan, G., Shi, S., Hao, C., Tang, Y., et al. (2020). Magnetic Ni/graphene connected with conductive carbon nano-onions or nanotubes by atomic layer deposition for lightweight and low-frequency microwave absorption. *Chem. Eng. J.* 382, 122980. doi:10.1016/j.cej.2019.122980

Xue, Y., Chen, S., Yu, J., Bunes, B. R., Xue, Z., Xu, J., et al. (2020). Nanostructured conducting polymers and their composites: Synthesis methodologies, morphologies and applications. *J. Mater. Chem. C* 8, 10136–10159. doi:10.1039/d0tc02152k

Yan, A., Lin, L., Na, S., Liu, C., and Wang, L. V. (2018). Large field homogeneous illumination in microwave-induced thermoacoustic tomography based on a quasi-conical spiral antenna. *Appl. Phys. Lett.* 113, 123701. doi:10.1063/1.5043541

Yan, M., Dai, J., and Qiu, M. (2014). Lithography-free broadband visible light absorber based on a mono-layer of gold nanoparticles. *J. Opt.* 16, 025002. doi:10.1088/2040-8978/16/2/025002

Yang, B., Fang, J., Xu, C., Cao, H., Zhang, R., Zhao, B., et al. (2022). *Nano-Micro Lett.* 14, 1–13.

Yang, B., Fang, J., Xu, C., Cao, H., Zhang, R., Zhao, B., et al. (2022). One-dimensional magnetic FeCoNi Alloy toward low-frequency electromagnetic wave absorption. *Nano-Micro Lett.* 14, 170. doi:10.1007/s40820-022-00920-7

Yang, H., Cao, X.-Y., Gao, J., Li, W., Yuan, Z., and Shang, K. (2013). *Prog. Electromagn. Res. M* 33, 31–44. doi:10.2528/pierm13080104

Yang, R.-B., Reddy, P. M., Chang, C.-J., Chen, P.-A., Chen, J.-K., and Chang, C.-C. (2016). Synthesis and characterization of Fe 3 O 4/polypyrrole/carbon nanotube composites with tunable microwave absorption properties: Role of carbon nanotube and polypyrrole content. *Chem. Eng. J.* 285, 497–507. doi:10.1016/j.cej.2015.10.031

Zhan, Y., Zhao, R., Xiang, X., He, S., Zhao, S., and Xue, W. (2019). Hierarchical core/shell bamboo-like polypyrrole nanofibers/Fe_3O_4 hybrids with superior microwave absorption performance. *Compos. Interfaces* 26, 1087–1100. doi:10.1080/09276440.2019.1586043

Zhang, C., Peng, Y., Song, Y., Li, J., Yin, F., and Yuan, Y. (2020). Periodic three-dimensional nitrogen-doped mesoporous carbon spheres embedded with Co/Co_3O_4 nanoparticles toward microwave absorption. *ACS Appl. Mater. interfaces* 12, 24102–24111. doi:10.1021/acsami.0c03105

Zhang, F., Cui, W., Wang, B., Xu, B., Liu, X., Liu, X., et al. (2021). Morphology-control synthesis of polyaniline decorative porous carbon with remarkable electromagnetic wave absorption capabilities. *Compos. Part B Eng.* 204, 108491. doi:10.1016/j.compositesb.2020.108491

Zhang, J., Wang, G., Zhang, B., He, T., He, Y., and Shen, J. (2016). Photo-excited broadband tunable terahertz metamaterial absorber. *Opt. Mater.* 54, 32–36. doi:10.1016/j.optmat.2016.02.011

Zhang, M., Cao, M.-S., Shu, J.-C., Cao, W.-Q., Li, L., and Yuan, J. (2021). Electromagnetic absorber converting radiation for multifunction. *Mater. Sci. Eng. R Rep.* 145, 100627. doi:10.1016/j.mser.2021.100627

Zhang, M., Qian, X., Zeng, Q., Zhang, Y., Cao, H., and Che, R. (2021). Hollow microspheres of polypyrrole/magnetite/carbon nanotubes by spray-dry as an electromagnetic synergistic microwave absorber. *Carbon* 175, 499–508. doi:10.1016/j.carbon.2021.01.013

Zhang, Z., Tan, J., Gu, W., Zhao, H., Zheng, J., Zhang, B., et al. (2020). Cellulose-chitosan framework/polyailine hybrid aerogel toward thermal insulation and microwave absorbing application. *Chem. Eng. J.* 395, 125190. doi:10.1016/j.cej.2020.125190

Zhang, Z., Zhang, L., Chen, X., Wu, Z., He, Y., Lv, Y., et al. (2020). Broadband metamaterial absorber for low-frequency microwave absorption in the S-band and C-band. *J. Magnetism Magnetic Mater.* 497, 166075. doi:10.1016/j.jmmm.2019.166075

Zhao, H.-B., Fu, Z.-B., Chen, H.-B., Zhong, M.-L., and Wang, C.-Y. (2016). Excellent electromagnetic absorption capability of Ni/carbon based conductive and magnetic foams synthesized via a green one pot route. *ACS Appl. Mater. interfaces* 8, 1468–1477. doi:10.1021/acsami.5b10805

Zhao, H., Cheng, Y., Lv, H., Ji, G., and Du, Y. (2019). A novel hierarchically porous magnetic carbon derived from biomass for strong lightweight microwave absorption. *Carbon* 142, 245–253. doi:10.1016/j.carbon.2018.10.027

Zhi, D., Li, T., Li, J., Ren, H., and Meng, F. (2021). A review of three-dimensional graphene-based aerogels: Synthesis, structure and application for microwave absorption. *Compos. Part B Eng.* 211, 108642. doi:10.1016/j.compositesb.2021.108642

Zhou, H., Pei, Z., Qu, S., Zhang, S., Wang, J., Li, Q., et al. (2009). A planar Zero-index metamaterial for directive Emission. *J. Electromagn. Waves Appl.* 23, 953–962. doi:10.1163/156939309788355289

Zhou, W., Li, K., Song, C., Hao, P., Chi, M., Yu, M., et al. (2015). Polarization-independent and omnidirectional nearly perfect absorber with ultra-thin 2D subwavelength metal grating in the visible region. *Opt. express* 23, A413–A418. doi:10.1364/oe.23.00a413

Zhou, X., Zhao, B., and Lv, H. (2022). *Nano Res.*, 1–10.

Zhou, Z., Chu, L., and Hu, S. (2006). Microwave absorption behaviors of tetra-needle-like ZnO whiskers. *Mater. Sci. Eng. B* 126, 93–96. doi:10.1016/j.mseb.2005.09.009

Zhou, Z., Yang, X., Zhang, D., Zhang, H., Cheng, J., Xiong, Y., et al. (2022). *Adv. Compos. Hybrid Mater.*, 1–11.

Zhou, Z., Yang, X., Zhang, D., Zhang, H., Cheng, J., Xiong, Y., et al. (2022). Achieving superior GHz-absorption performance in VB-group laminated VS2 microwave absorber with dielectric and magnetic synergy effects. *Adv. Compos. Hybrid Mater.* 5, 2317–2327. doi:10.1007/s42114-022-00416-3

Zhuo, R., Qiao, L., Feng, H., Chen, J., Yan, D., Wu, Z., et al. (2008). Microwave absorption properties and the isotropic antenna mechanism of ZnO nanotrees. *J. Appl. Phys.* 104, 094101. doi:10.1063/1.2973198